DENDRITIC CELLS

Arc/Arg3.1 governs inflammatory dendritic cell migration from the skin and thereby controls T cell activation

Friederike Ufer,[1] Pablo Vargas,[2]* Jan Broder Engler,[1]* Joseph Tintelnot,[1] Benjamin Schattling,[1] Hana Winkler,[1] Simone Bauer,[1] Nina Kursawe,[1] Anne Willing,[1] Oliver Keminer,[3] Ora Ohana,[4] Gabriela Salinas-Riester,[5] Ole Pless,[3] Dietmar Kuhl,[4] Manuel A. Friese[1]†

Skin-migratory dendritic cells (migDCs) are pivotal antigen-presenting cells that continuously transport antigens to draining lymph nodes and regulate immune responses. However, identification of migDCs is complicated by the lack of distinguishing markers, and it remains unclear which molecules determine their migratory capacity during inflammation. We show that, in the skin, the neuronal plasticity molecule activity-regulated cytoskeleton-associated protein/activity-regulated gene 3.1 (Arc/Arg3.1) was strictly confined to migDCs. Mechanistically, Arc/Arg3.1 was required for accelerated DC migration during inflammation because it regulated actin dynamics through nonmuscle myosin II. Accordingly, Arc/Arg3.1-dependent DC migration was critical for mounting T cell responses in experimental autoimmune encephalomyelitis and allergic contact dermatitis. Thus, Arc/Arg3.1 was restricted to migDCs in the skin and drove fast DC migration by exclusively coordinating cytoskeletal changes in response to inflammatory challenges. These findings commend Arc/Arg3.1 as a universal switch in migDCs that may be exploited to selectively modify immune responses.

INTRODUCTION

Host defense mechanisms have evolved to detect and eliminate invading pathogens and malignant cells, while at the same time remaining tolerant to self-, commensal, and environmental antigens (*1*). At the host-environment interfaces, dendritic cells (DCs) continuously sense and interpret surrounding cues and instruct T and B cells to initiate an adaptive immune response or tolerance to presented antigens (*2*). Accordingly, DCs are involved in most autoimmune and allergic diseases, as implicated by human studies and experimental models (*3*, *4*).

To constantly sample and transport antigens from peripheral tissues to draining lymph nodes (dLNs), skin-resident immature DCs undergo permanent homeostatic maturation, even in the absence of pathogens (*5*, *6*). With maturation, skin-migratory DCs (migDCs) change their morphology, cytokine secretion, and major histocompatibility complex (MHC) class II and costimulatory molecule expression at the cell surface (*7*). Within the skin-DC network, at least four distinct migDC subsets, including the epidermal Langerhans cells (LCs), have been identified and recently shown to selectively promote different immune responses to manifold environmental and "self" challenges (*8*, *9*). However, during inflammation, large numbers of migDCs rapidly mature and accelerate migration through the tissue and lymphatics and eventually enter dLNs to interact with T cells for antigen presentation (*10*). This migDC–T cell interaction is key to either induce effector immune responses or confer tolerance. This is reflected in the animal model of multiple sclerosis (*11*), experimental autoimmune encephalomyelitis (EAE), in which rare encephalitogenic $CD4^+$ T cells encounter their cognate antigen on DCs in the dLN after myelin-associated antigen immunization (*12*, *13*). These T cells then drive inflammation and tissue damage in the central nervous system (CNS). Similarly, small organic molecules (haptens) can react with self-proteins and generate immunogenic neoantigens, which are transported by skin-DCs to dLNs, where they activate T cells. Reencounter of these haptens recruits activated effector T cells to the site of antigen encounter in the skin, which clinically presents as allergic contact dermatitis (*4*, *14*).

However, these responses can only be generated if DCs properly migrate from peripheral tissues to dLNs to adequately deliver and communicate self- and foreign antigens, together with appropriate anti- and pro-inflammatory signals. Despite recent progress, substantial gaps in our understanding of DC locomotion still exist (*7*). It remains unclear how DCs reorganize their actin cytoskeleton to facilitate fast migration in response to inflammatory stimuli and which molecules instruct this reorganization. In addition, the lack of specific surface markers to definitely identify functionally different DC subsets complicates DC research (*15*, *16*). However, unequivocal identification of fast-migrating migDCs during inflammation would allow one to understand their complex behavior and to eventually target them in autoimmunity, allergy, vaccination, or cancer therapy (*5*, *16*, *17*).

It has been reported that cytoskeletal coordination during DC locomotion resembles that of migrating neurons during development (*18*, *19*). In addition, both adult neurons and DCs constantly reorganize their actin cytoskeleton, which is reflected by on-demand modification of their manifold protrusions (*7*, *20*). Hence, it is conceivable that both cell types might share similar principles of coordinating cell shape in response to changing environmental cues. In this context, activity-regulated cytoskeleton-associated protein/activity-regulated gene 3.1 (Arc/Arg3.1) has been described as a critical regulator of neuronal plasticity that is involved in rearrangement of neuronal dendritic spines (*21*, *22*). However, the expression of

[1]Institut für Neuroimmunologie und Multiple Sklerose, Zentrum für Molekulare Neurobiologie Hamburg, Universitätsklinikum Hamburg-Eppendorf, 20251 Hamburg, Germany. [2]Institut Curie, PSL Research University, CNRS, UMR 144, 75005 Paris, France. [3]Fraunhofer-Institut für Molekularbiologie und Angewandte Oekologie IME, ScreeningPort, 22525 Hamburg, Germany. [4]Institut für Molekulare und Zelluläre Kognition, Zentrum für Molekulare Neurobiologie Hamburg, Universitätsklinikum Hamburg-Eppendorf, 20251 Hamburg, Germany. [5]Microarray and Deep-Sequencing Core Facility, Universitätsmedizin Göttingen, 37077 Göttingen, Germany.
*These authors contributed equally to this work.
†Corresponding author. Email: manuel.friese@zmnh.uni-hamburg.de

Arc/Arg3.1 was assumed to be tightly restricted to neurons of the CNS, and Arc/Arg3.1 has not been reported to be involved in neuronal migration (*23*, *24*).

In this study, we identified Arc/Arg3.1 exclusively in migDCs and proposed a previously unknown strategy to functionally identify migrating DCs via their stable expression of Arc/Arg3.1. In addition, we could show that Arc/Arg3.1 is instrumental for fast DC migration in vitro and in vivo by facilitating intracellular actin turnover in response to inflammatory stimuli by acting on myosin II (MyoII). Consequently, Arc/Arg3.1 activity in migDCs directly determined the extent of autoreactive T cell activation in dLNs in EAE and in delayed-type skin hypersensitivity reactions.

RESULTS

Arc/Arg3.1 is exclusively expressed in migDCs

To investigate whether the to date only neuronally reported molecule Arc/Arg3.1 has a role in immune cells, we assessed its expression in mouse skin and lymphoid organs. We observed substantial *Arc/Arg3.1* mRNA expression in the skin and skin-draining LN (sdLN) but not in the spleen (Fig. 1A), a pattern suggestive of tissue-patrolling DCs (*16*). Arc/Arg3.1 mRNA and protein were present in isolated DCs and bone marrow–derived DCs (BMDCs) but not in other immune cell populations (Fig. 1, B and C, and fig. S1A). Furthermore, analysis of DC subsets showed that Arc/Arg3.1 expression was restricted to migDCs, whereas expression was absent in conventional DCs (cDCs) and plasmacytoid DCs (pDCs) (Fig. 1, D and E).

To further substantiate this finding, we used a bacterial artificial chromosome transgenic reporter mouse that expresses enhanced green fluorescent protein (eGFP) driven by the *Arc/Arg3.1* promoter (*Arc/Arg3.1*^{eGFP}) (*25*). Consistent with our mRNA and protein analyses, the *Arc/Arg3.1*-eGFP signal was exclusively detected in migDCs (Fig. 1F), and all *Arc/Arg3.1*-eGFP$^+$ cells fell into the migDC gate (Fig. 1G). Within the Arc/Arg3.1-eGFP$^+$ migDCs, we found CD11b$^+$, CD103$^+$, XCR1$^+$, and CD8$^+$ DCs but only negligible amounts of CD64$^+$ or Ly6G/C$^+$ cells, with the latter being indicative of monocytes or macrophages (fig. S1B). Consistently, *Arc/Arg3.1* mRNA was detectable in migDC subpopulations, that is, CD11b$^+$, CD103$^+$, and LCs (fig. S1C). Moreover, all Arc/Arg3.1$^+$ DCs showed homogenous and markedly elevated expression of CCR7, CD40, and CD86 in comparison to other DCs (all $P < 0.001$; Fig. 1H), which is in accordance with a migDC phenotype (*5*, *6*). We concluded that Arc/Arg3.1 expression in the immune system is a unique property of migDCs.

Arc/Arg3.1 functionally defines migDCs

Next, we investigated whether Arc/Arg3.1 expression is restricted to cells that not only resemble migrating DCs in terms of surface markers but also by function. *Arc/Arg3.1* mRNA was undetectable in sdLN DCs when we disabled migDCs from entering sdLNs by genetic disruption of the chemokine receptor CCR7 (Fig. 2, A and B) (*26*). *Arc/Arg3.1* expression in BMDCs of *Ccr7*-deficient mice was readily detectable, indicating that a reduced influx of migrating DCs, but not their inability to express Arc/Arg3.1, led to this result (Fig. 2B). To pharmacologically disrupt steady-state migration into sdLNs at a given time point, we orally administered the functional sphingosine 1-phosphate receptor antagonist fingolimod (FTY720), which impairs DC influx into LNs (*27*) and is a drug approved by the U.S. Food and Drug Administration and the European Medicines Agency for multiple sclerosis treatment (*11*, *28*). Consistently treating wild-type

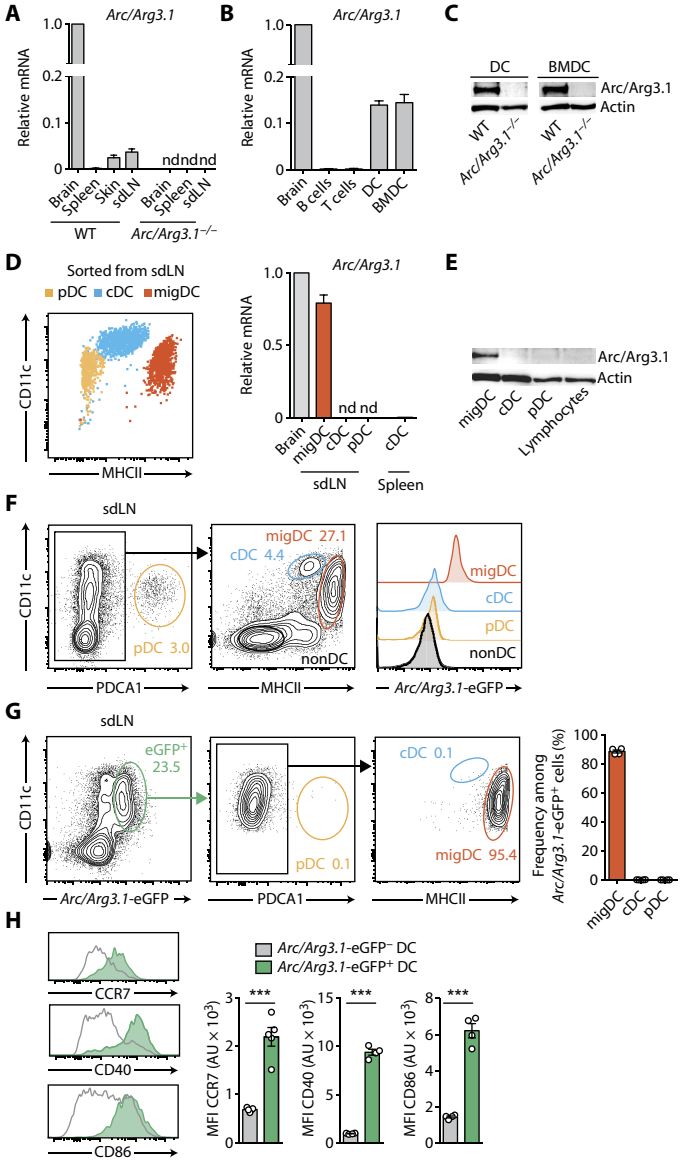

Fig. 1. Arc/Arg3.1 is exclusively expressed in migDCs. (**A**) Relative *Arc/Arg3.1* mRNA expression in indicated organs ($n = 3$). Mean ± SEM; nd, not detected. (**B**) Relative *Arc/Arg3.1* mRNA expression in indicated sorted cell samples of WT mice. Pooled data from three independent experiments. There are 6 to 10 WT mice per sorted cell sample. Mean ± SEM. (**C**) Immunoblot of Arc/Arg3.1 from sorted DCs of sdLNs and BMDCs. Data from one of three experiments. (**D**) Analysis of flow cytometry–sorted DC subsets from sdLNs and relative *Arc/Arg3.1* mRNA of flow cytometry–sorted DC subsets from the sdLN and spleen. Pooled data from four independent experiments. There are 6 to 10 WT mice per sorted cell sample. Mean ± SEM. (**E**) Immunoblot of Arc/Arg3.1 protein in DC subsets and lymphocytes from sdLNs. Data from one of three experiments. (**F**) Gating strategy for DC subset analysis from sdLNs and *Arc/Arg3.1*-eGFP expression in DC subsets of *Arc/Arg3.1*^{eGFP} mice. (**G**) Representative flow cytometry analysis of *Arc/Arg3.1*-eGFP$^+$ cells from sdLNs of *Arc/Arg3.1*^{eGFP} mice and quantification ($n = 4$). Data from one of three experiments. Mean ± SEM. (**H**) Median fluorescence intensity (MFI) of CCR7, CD40, and CD86 in *Arc/Arg3.1*-eGFP$^+$ and *Arc/Arg3.1*-eGFP$^-$ DCs from sdLNs of *Arc/Arg3.1*^{eGFP} mice ($n = 4$ to 5). Mean ± SEM. Data from one of three experiments. Two-tailed Student's *t* test; ***$P < 0.001$. AU, arbitrary units.

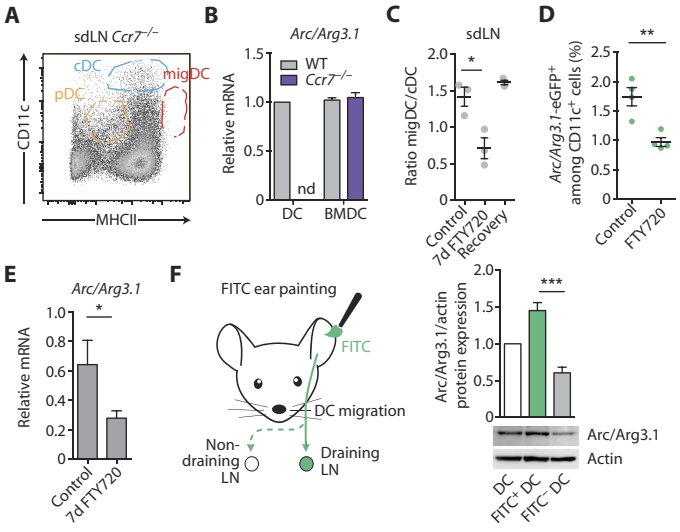

Fig. 2. Arc/Arg3.1 functionally defines migrating DCs. (**A**) Flow cytometry analysis of DC subsets from sdLNs of *Ccr7*$^{-/-}$ mice. (**B**) Relative *Arc/Arg3.1* mRNA of DCs from sdLNs and BMDCs (n = 3) of WT and *Ccr7*$^{-/-}$ mice. Data from one of two experiments. Mean ± SEM. (**C**) Ratio of migDCs to cDCs in sdLNs of WT mice by flow cytometry at baseline (control), after 7 days of FTY720 treatment or 7 days after treatment discontinuation (recovery) (n = 3 each). Data from one of four experiments. Bars represent mean ± SEM. Two-tailed Student's t test; *P < 0.05. (**D**) Frequency of *Arc/Arg3.1*-eGFP$^+$ cells in sdLNs at baseline (control) and after treatment with FTY720 (n = 4 each time point). Data from one of two experiments. Bar represent mean ± SEM. Two-tailed Student's t test; **P < 0.01. (**E**) Relative *Arc/Arg3.1* mRNA expression in sdLNs of WT mice before and after 7 days of FTY720 treatment (n = 14 each time point). Pooled data from three experiments. Mean ± SEM. Two-tailed Student's t test; *P < 0.05. (**F**) Immunoblot of Arc/Arg3.1 from recently migrated DCs (FITC$^+$) and of LN-resident DCs (FITC$^-$) from dLNs after FITC skin painting and densitometric quantification normalized to actin. Pooled data from four experiments. There are five to eight WT mice per sorted cell sample. Mean ± SEM. Two-tailed Student's t test; ***P < 0.001.

(WT) and *Arc/Arg3.1*^{eGFP} mice with FTY720 led to a 50% reduction of migDC frequency in sdLNs, which recovered after FTY720 discontinuation (P = 0.02; Fig. 2C). At the same time, FTY720 treatment significantly reduced *Arc/Arg3.1*-eGFP$^+$ DCs as well as *Arc/Arg3.1* mRNA in sdLNs [P = 0.004 (Fig. 2D), P = 0.04 (Fig. 2E)].

To pinpoint the fact that Arc/Arg3.1 expression functionally characterizes DCs that migrate from environmental interfaces into LNs, we used a skin contact sensitization model. After applying an organic solvent containing fluorescein isothiocyanate (FITC) on the ears of mice (*26*), recently migrated FITC$^+$ DCs showed significantly higher Arc/Arg3.1 protein content in comparison to resident FITC$^-$ DCs in dLNs (P < 0.001; Fig. 2F). Hence, we hypothesized that Arc/Arg3.1 expression might itself be involved in regulating migration.

DCs rely on Arc/Arg3.1 for fast inflammatory migration

To test whether DCs rely on the Arc/Arg3.1 protein function for steering migration, we used *Arc/Arg3.1*-deficient mice, which showed no a priori dysregulation of their peripheral immune cell composition (CD4$^+$ and CD8$^+$ T cells, natural killer and natural killer T cells, B cells, neutrophils, and macrophages) in steady state or 3 days after subcutaneous inflammatory challenge with complete Freund's adjuvant (CFA; fig. S2, A and B). However, during CFA-induced inflammation, skin-descending CD103$^+$ DCs were profoundly reduced among migDCs in dLNs of *Arc/Arg3.1*$^{-/-}$ mice compared to WT controls (P = 0.002; Fig. 3A), whereas the other major migDC subsets LC and CD11b$^+$ (*8*) were unaffected by *Arc/Arg3.1* deficiency (fig. S2C). Notably, in the contact sensitization model, the frequency of recently migrated DCs was drastically reduced in *Arc/Arg3.1*$^{-/-}$ mice to about one-fifth of WT controls (P < 0.001; Fig. 3B). We ruled out fundamentally impaired DC development by analyzing frequencies of DC progenitors in the bone marrow (*29*) because we detected no differences in macrophage DC progenitors (lineage$^-$CD115$^+$CD135$^+$CD117^{high}) and common DC progenitors (lineage$^-$CD115$^+$CD135$^+$CD117^{low}) between *Arc/Arg3.1*$^{-/-}$ and WT mice (fig. S2D). Moreover, CCR7 surface expression was unaltered in total migDCs or specifically CD103$^+$ migDCs from sdLNs of *Arc/Arg3.1*$^{-/-}$ mice compared to WT littermate controls (Fig. 3C). We also did not detect a significant reduction of skin-resident DCs (fig. S2E). Therefore, we concluded that *Arc/Arg3.1*$^{-/-}$ DCs show a migratory defect.

To investigate which specific aspect of migration is disturbed upon Arc/Arg3.1 disruption, we analyzed the motility of BMDCs by time-lapse imaging in microfabricated channels (*30*). We used BMDCs because they show migratory activity (*18*, *30*), closely cluster with migDCs on a transcriptional level (*31*), and express Arc/Arg3.1 (Fig. 1, B and C). Notably, BMDCs from WT and *Arc/Arg3.1*$^{-/-}$ mice displayed a similar instantaneous velocity. However, WT BMDCs activated with lipopolysaccharide (LPS) exhibited a strong increase in migration speed (P < 0.001). By contrast, *Arc/Arg3.1*$^{-/-}$ BMDCs failed to increase migration speed upon activation (P < 0.001; Fig. 3D). We could exclude differences between *Arc/Arg3.1*$^{-/-}$ and WT BMDCs in respect of antigen uptake as measured by FITC-dextran ingestion (fig. S3A), LPS-induced maturation (MHC class II expression; fig. S3B) and activation (CD40, CD80, CD86, and CCR7 expression; fig. S3C), and calcium signaling (fig. S3D).

To directly compare migratory capacity in vivo, we loaded LPS-activated BMDCs of *Arc/Arg3.1*$^{-/-}$ and WT mice with different fluorescent dyes and injected them as an equal mix into the footpad of WT mice. Significantly less *Arc/Arg3.1*$^{-/-}$ BMDCs compared with WT BMDCs arrived at the draining popliteal LN (P < 0.001; Fig. 3, E and F). Accordingly, when injecting BMDCs from *Arc/Arg3.1*^{eGFP} mice in WT recipients, the fraction of recovered Arc/Arg3.1$^+$ DCs increased more than twofold in comparison to the fraction of Arc/Arg3.1$^+$ DCs in the initial input (P < 0.01; Fig. 3G). Thus, we define an important function of Arc/Arg3.1 in controlling DC migratory properties under inflammatory conditions.

Arc/Arg3.1 shapes DC morphology

Because Arc/Arg3.1 is crucially involved in neuronal homeostasis and plasticity, processes that involve direct changes in actin dynamics (*21*, *22*), we assessed the impact of Arc/Arg3.1 on the cytoskeletal machinery in DCs. We conducted phenotypic high-content screening monitoring morphology parameters in DCs in response to different inflammatory stimuli and observed alterations in cell size and shape of *Arc/Arg3.1*$^{-/-}$ BMDCs after LPS stimulation (Fig. 4A). Detailed analysis in validation experiments revealed that, whereas LPS-activated WT BMDCs presented as irregularly shaped cells with multiple protrusions, *Arc/Arg3.1*$^{-/-}$ BMDCs appeared as rather uniform cells with reduced area and decreased protrusions, which resulted in rounder cells with markedly reduced volume (P < 0.001 for all; Fig. 4, B and C). Notably, in analogy to our in vitro data, epidermal LCs analyzed in epidermal sheets from ear skin were

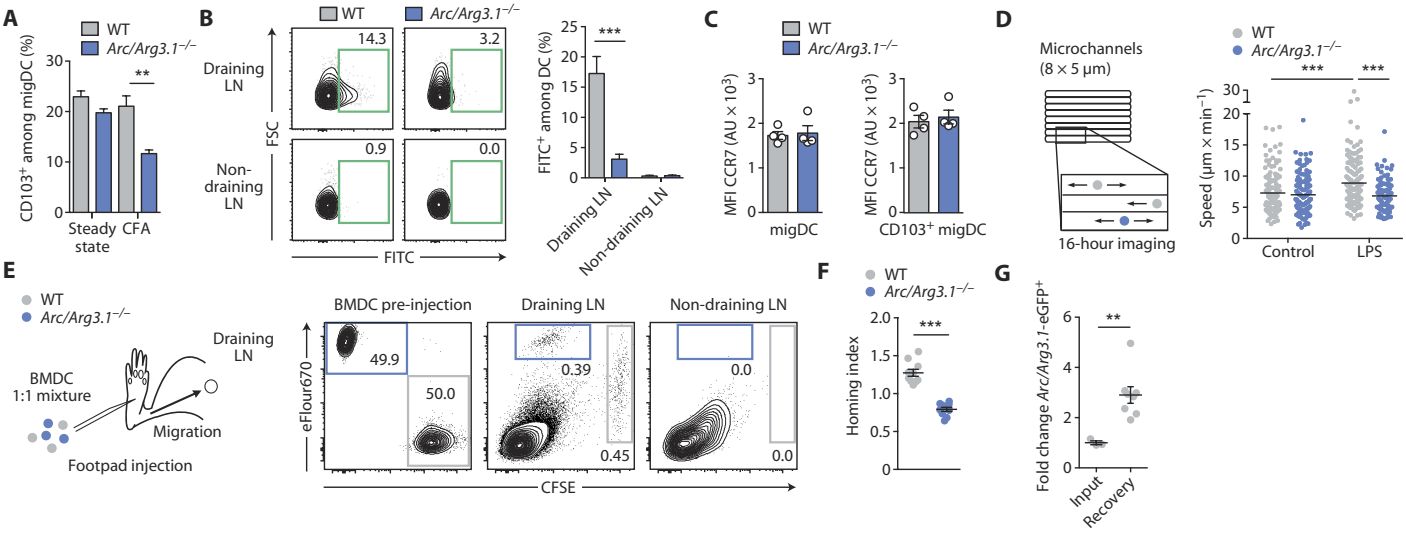

Fig. 3. Arc/Arg3.1 is required for fast inflammatory DC migration. (**A**) Flow cytometry analysis of CD103$^+$ DCs among migDCs in sdLNs in steady state and inflammation (3 days after CFA with $MOG_{35–55}$ subcutaneously; $n = 5$ per group). Data from one of three experiments. Mean ± SEM. Two-tailed Student's t test; $^{**}P < 0.01$. (**B**) Flow cytometry analysis of FITC$^+$ DCs in dLNs and nondraining LNs after FITC ear-skin painting. Bar plot shows FITC$^+$ DCs for WT and *Arc/Arg3.1*$^{-/-}$ ($n = 7$ per group) mice. Data from one of three experiments. Mean ± SEM. Two-tailed Student's t test; $^{***}P < 0.001$. (**C**) Flow cytometry analysis of CCR7 MFI on migDC and CD103$^+$ among migDCs isolated from sdLNs of WT and *Arc/Arg3.1*$^{-/-}$ mice ($n = 4$ per group). Data from one of two experiments. Mean ± SEM. Two-tailed Student's t test. (**D**) Mean migration speed of control and LPS-activated BMDCs in microchannels. Bars represent mean. Data from one of three experiments. Mann-Whitney test; $^{***}P < 0.001$. (**E** and **F**) Differently labeled WT and *Arc/Arg3.1*$^{-/-}$ BMDCs were injected into the footpad of WT mice at a ratio of 1:1 and recovered from popliteal LNs. An example of WT BMDCs labeled with CFSE and *Arc/Arg3.1*$^{-/-}$ BMDCs labeled with eFlour670 is shown. Homing index shows relative recovery for each genotype ($n = 10$ each) (F). Data from one of three experiments. Mean ± SEM. Two-tailed Student's t test; $^{***}P < 0.001$. (**G**) Labeled BMDCs from *Arc/Arg3.1*^{eGFP} mice ($n = 3$) were injected in the footpad of WT mice ($n = 8$). Frequency of *Arc/Arg3.1*-eGFP$^+$ cells was determined in the input and recovered popliteal LN by flow cytometry. Two-tailed Student's t test; $^{**}P < 0.01$.

significantly reduced in size and perimeter that goes along with an increased circularity in *Arc/Arg3.1*$^{-/-}$ mice in comparison to WT mice (all $P < 0.001$; Fig. 4D). In addition, *Arc/Arg3.1*$^{-/-}$ BMDCs showed a marked defect in adhesion ($P < 0.001$ for bovine fibronectin and $P = 0.004$ for human fibronectin; Fig. 4E) that transduced to less RhoA activation ($P = 0.04$; Fig. 4F) (*32*), although BMDCs from both genotypes were equipped with equal levels of surface integrins (CD29 and CD49e; fig. S4, A and B). Both findings are suggestive of disturbed actin remodeling in the absence of Arc/Arg3.1.

Arc/Arg3.1 regulates intracellular actin dynamics via nonmuscle MyoII

To further decipher the role of Arc/Arg3.1 in DC migration on a subcellular level, we first interrogated gene expression changes of BMDCs of respective genotypes. Only 45 gene transcripts were differentially regulated in a gene array of *Arc/Arg3.1*$^{-/-}$ and WT BMDCs (table S1), whereas among these gene transcripts, only *Arc/Arg3.1* itself was associated with the Gene Ontology (GO) term "locomotion" (Fig. 5A). An additional gene array after LPS stimulation of BMDC did not reveal any further, differently regulated genes (table S1), nor was Arc/Arg3.1 itself induced by LPS or other pathogen [polyinosinic:polycytidylic acid (polyI:C)], danger, and inflammatory signals [adenosine triphosphate (ATP), calcium, glutamate, CCL19, CCL21, and tumor necrosis factor–α (TNF-α); fig. S5, A and B]. Likewise, *Arc/Arg3.1* mRNA remained absent in LN-resident cDCs or pDCs after in vivo CFA application or ex vivo treatment of isolated splenic cDCs with LPS or polyI:C (fig. S5, C and D). Because we did not see any transcriptional change in *Arc/Arg3.1* levels upon stimulation, we determined whether, in analogy to its neuronal function as an immediate-early gene (*21*), a rapid translation of *Arc/Arg3.1* mRNA might lead to an increase in protein level. Immunoblot analysis did not reveal rapid changes in Arc/Arg3.1 protein expression after LPS activation (fig. S5E), and in total, we could not find evidence for Arc/Arg3.1 acting as a cytoskeletal regulator via changes in expression.

Therefore, we directly assessed actin remodeling during cell locomotion by staining filamentous actin (F-actin) with phalloidin during spontaneous migration (*30*). We performed our analyses in confined microchannels, which result in an amoeboid migration that is irrespective of dendritic protrusions (*18*). In this system, cells acquire the shape of the tubes into which they migrate, allowing comparisons of polymerized actin distribution (*33*). In our setup, we analyzed actin distribution in superimposed static images (>20 cells) to evidence general changes in actin distribution. We observed highly concentrated F-actin at the cell front in BMDCs of both genotypes (Fig. 5B). However, although LPS activation induced a rearrangement of actin toward the cell rear in WT BMDCs, this actin polymerization was abolished in *Arc/Arg3.1*$^{-/-}$ BMDCs (both $P < 0.001$; Fig. 5B).

One of the key proteins involved in actin polymerization and depolymerization is cofilin. In migrating cells, cofilin is active at the leading edge of locomotor protrusions, and inhibition of its activity causes defects in protrusion, cell polarity, and migration (*34*). Arc/Arg3.1 has been proposed to modulate cofilin phosphorylation in neurons (*22*). However, we could not detect any difference in cofilin phosphorylation in BMDCs in the absence of Arc/Arg3.1 (fig. S5F).

Because translocation of MyoII to the cell rear is responsible for fast locomotion in DCs (*35*), we next determined whether MyoII activity is equally disturbed in *Arc/Arg3.1*$^{-/-}$ DCs. After activation with LPS, phosphorylated MyoII showed a marked increase in WT

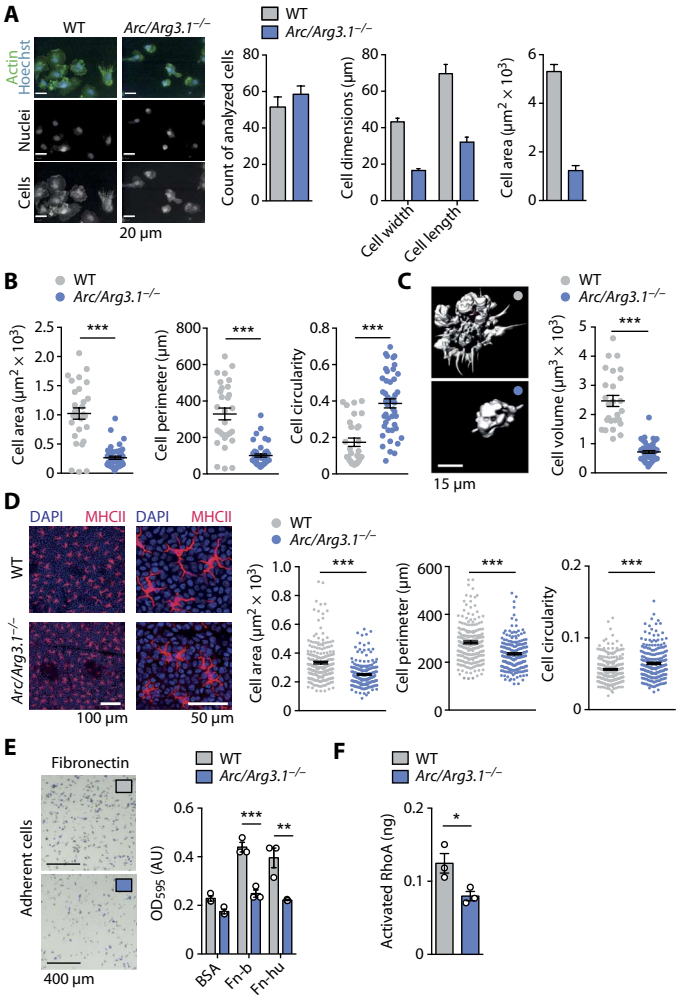

Fig. 4. Arc/Arg3.1 shapes DC morphology. (**A**) BMDC phenotype screening with images of LPS-activated BMDCs and automated recognition of cell nuclei and cell body (left). Quantification of cell numbers, width, length, and area (right). Mean ± SEM. No statistics were applied; results were independently validated in (**B**). Phalloidin-stained BMDCs (B) were analyzed for area (left), perimeter (middle), and circularity (right). Data from one of three experiments, each with BMDCs from three animals per genotype. Mean ± SEM. Two-tailed Student's *t* test; ***$P < 0.001$. (**C**) Z-stack images of phalloidin-stained BMDCs were analyzed for cell volume. Data from one of three experiments, each with BMDCs from three animals per genotype. Mean ± SEM. Two-tailed Student's *t* test; ***$P < 0.001$. (**D**) Representative immunostaining of LCs ($MHCII^+$) in epidermal sheets taken from ear skin of WT and *Arc/Arg3.1*$^{-/-}$ mice (left). Statistical analysis of LC area, perimeter, and circularity is shown (right). Data from one of two experiments, each with pooled data from three different animals per genotype. Mean ± SEM. Two-tailed Student's *t* test; ***$P < 0.001$. (**E**) Representative images and optical density analysis of fibronectin-adherent BMDCs. Data from one of three experiments, each with BMDCs from three animals per genotype. Two-tailed Student's *t* test; **$P < 0.01$, ***$P < 0.001$. Fn-b, bovine fibronection; Fn-hu, human fibronection. (**F**) Activated RhoA was assessed by ELISA in BMDC after adhesion to fibronectin. Data from one of two experiments, each with BMDCs from three animals per genotype. Mean ± SEM. Two-tailed Student's *t* test; *$P < 0.05$.

BMDCs that was abrogated in *Arc/Arg3.1*$^{-/-}$ BMDCs, as recorded by flow cytometry ($P = 0.008$; Fig. 5C). Treatment of WT BMDCs with blebbistatin, an adenosine triphosphatase inhibitor of MyoII, abolished the increase in migratory speed after LPS activation, thereby mimicking the phenotype of *Arc/Arg3.1*$^{-/-}$ BMDCs ($P < 0.001$; Fig. 5D). Blebbistatin treatment of *Arc/Arg3.1*$^{-/-}$ BMDCs showed no additional inhibitory effect on migratory speed. Together, these findings demonstrate a nontranscriptional regulation of Arc/Arg3.1 of MyoII-dependent actin dynamics that facilitate fast DC migration.

Arc/Arg3.1 has a functional impact on T cell stimulation and EAE

Next, we determined to which extent skin-DCs rely on Arc/Arg3.1-dependent migration to mount autoantigen-specific T cell responses by subcutaneously immunizing mice with myelin oligodendrocyte glycoprotein peptide 35–55 ($MOG_{35–55}$) in mycobacteria-based CFA to initiate EAE, the animal model of multiple sclerosis (*36*).

Arc/Arg3.1$^{-/-}$ mice showed a significantly ameliorated EAE disease course ($P = 0.04$; Fig. 6A) with reduced maximum disease score ($P = 0.002$; Fig. 6B) and reduced loss of body weight ($P = 0.04$; Fig. 6C) as well as substantially reduced infiltrating immune cells in the CNS at day 12 after immunization in comparison to WT littermate controls ($P = 0.02$; Fig. 6D and fig. S6A). Consistently, in dLNs, immune cell counts that primarily consist of clonally expanded T cells were reduced ($P = 0.02$; Fig. 6E), and $MOG_{35–55}$-specific T cell recall response was attenuated in the absence of *Arc/Arg3.1* [$P = 0.007$ for $MOG_{35–55}$ (10 µg ml^{-1}); Fig. 6F]. Because T cell responsiveness was not altered when antibodies directed against CD3 were used, we could exclude a T cell–intrinsic defect in *Arc/Arg3.1*$^{-/-}$ mice (Fig. 6F). In addition, WT and *Arc/Arg3.1*$^{-/-}$ BMDCs showed the same capacity to stimulate $MOG_{35–55}$-specific T cell receptor (2D2) transgenic $CD4^+$ T cells (*37*) in vitro (fig. S6B). Thus, in vivo defective Arc/Arg3.1-dependent skin-DC migration leads to an amelioration of EAE, because $MOG_{35–55}$-specific T cell priming in the draining inguinal LN is reduced in the absence of *Arc/Arg3.1*. This leads to less $CD4^+$ T cell proliferation in the inguinal LN before EAE onset, and finally results in less leukocyte infiltration in the CNS at the peak of EAE severity.

Arc/Arg3.1 controls DC-driven allergic contact dermatitis

After having established the importance of Arc/Arg3.1-dependent skin-DC migration for mounting an immune response in the EAE model, we lastly analyzed the importance of our finding in a model of allergic contact dermatitis, which is highly dependent on skin-DC migration. We topically applied the hapten FITC to the abdominal skin of WT or *Arc/Arg3.1*$^{-/-}$ mice from which it is transported by migratory skin-DCs to the sdLNs where they induce a hapten-specific T cell response (*4*, *14*). After reapplying FITC to one ear 5 days later, we estimated the generation of hapten-specific effector T cells by measuring ear swelling reactions in comparison to the unchallenged contralateral ear. Ear swelling as a measure of delayed-type hypersensitivity reaction was massively reduced in *Arc/Arg3.1*$^{-/-}$ mice in comparison to WT littermate control mice ($P < 0.001$; Fig. 7, A and B). The reduced ear swelling in *Arc/Arg3.1*$^{-/-}$ mice was accompanied by reduced lymphocyte numbers in draining cervical LNs ($P = 0.009$; Fig. 7C). Hence, inflammatory skin-DC migration is highly dependent on Arc/Arg3.1 function.

DISCUSSION

Here, we show that, in the skin, Arc/Arg3.1 plays a key role in the immune system where it exclusively identifies migDCs. Furthermore, we demonstrate that Arc/Arg3.1 is critical for fast DC migration after

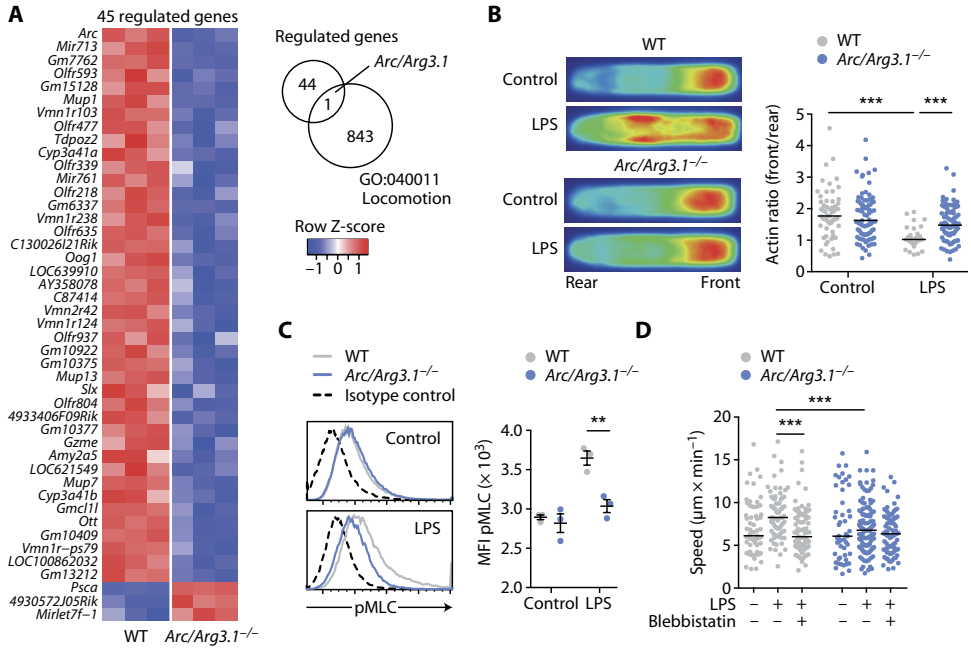

Fig. 5. Arc/Arg3.1 influences actin dynamics in migration. (**A**) Gene array of WT and *Arc/Arg3.1*$^{-/-}$ BMDCs (n = 3 per genotype). Moderated t test corrected for multiple comparisons via the Benjamini-Hochberg method. (**B**) Mean actin distribution from migrating BMDCs (>20 cells per condition as superimposed projection). Scatter plot shows actin ratio (front to rear) for individual cells. Data from one of two experiments. Mann-Whitney test; ***P < 0.001. (**C**) MFI of phosphorylated MyoII in BMDCs after LPS stimulation acquired by flow cytometry. Data from one of two experiments, each with BMDCs from three animals per genotype. Two-tailed Student's t test; **P < 0.01. pMLC, phosphomyosin light chain. (**D**) Mean migration speed of BMDCs in the presence of LPS and/or blebbistatin in microchannels. Data from one of two experiments. Mann-Whitney test; ***P < 0.001.

inflammatory activation in vitro and in vivo. Mechanistically, the morphologic phenotype revealed disrupted cytoskeletal architecture with markedly reduced protrusions in the absence of Arc/Arg3.1. On a subcellular level, detailed analysis of actin dynamics during actual DC migration revealed a decreased actin polymerization that was accompanied by less phosphorylation of MyoII. In preclinical models, we provide evidence that the impaired fast DC migration in response to inflammatory signals resulted in insufficient T cell priming, which is reflected in an ameliorated EAE disease course of *Arc/Arg3.1*$^{-/-}$ mice and less skin contact hypersensitivity reaction (see graphical summary; fig. S7).

Our results of diminished dendrites in *Arc/Arg3.1*$^{-/-}$ DCs favor the notion that, beyond appearance, both neurons and migDCs rely on Arc/Arg3.1 in forming their elaborate branches (*38*). These protrusions largely consist of actin bundles, and Arc/Arg3.1 has been hypothesized to influence actin dynamics in neuronal dendrites (*21*), but Arc/Arg3.1 has never been reported to regulate migration of neurons. Notably, we found that actin-dependent spatial contractility was severely disturbed in DCs in the absence of *Arc/Arg3.1*, with an abrogated intracellular actin polymerization at the cell rear that is important to increase migratory speed after activation with LPS (*33*). In neurons, acute inhibition of Arc/Arg3.1 synthesis induces dephosphorylation of cofilin to facilitate actin-dependent glutamate receptor trafficking during synaptic plasticity (*22*). However, in DCs, we did not detect Arc/Arg3.1-dependent cofilin phosphorylation after LPS treatment but, instead, demonstrated that Arc/Arg3.1 regulates DC migration speed via MyoII phosphorylation and its actomyosin coupling (*39*).

DCs deficient in genes that regulate actin dynamics or network architecture, such as the Rho guanosine triphosphatases Rac1, Rac2, and Cdc42 or the Wiskott-Aldrich syndrome protein (WASp), formin mammalian Diaphanous-related 1 (mDia), Dedicator of cytokinesis 8 (DOCK8), or the actin-nucleating complex Arp2/3, impair all modes of DC migration (*40*). Moreover, these proteins are abundantly expressed in other migrating immune cell populations and show no exclusivity for DC migration. Although other proteins such as Eps8 (*41*) or fascin-1 (*42*) are less abundant in other immune cells, they are still not exclusive to migDCs. By contrast, Arc/Arg3.1 determines the transition from steady state to fast DC locomotion during inflammation and is highly specific for migDCs. Together with the observation that Arc/Arg3.1 was not inducible in other DCs, such as LN- or spleen-resident cDCs, upon inflammatory challenge, this suggests a context-dependent functional specialization of the different skin-DC subsets or possibly a unique ontogeny of migDCs.

We also demonstrate that the presence of Arc/Arg.3.1 at steady state or after LPS activation does not result in transcriptional changes, implying that the Arc/Arg.3.1-dependent transition to fast migration does not require a change in the genetic program of migrating DCs. Therefore, Arc/Arg3.1 acts as an immediate switch in migDCs to quickly change their morphodynamic modes in response to changing environmental cues.

Because we found that inflammatory DC migration in vivo and in vitro is massively impaired in the absence of Arc/Arg3.1, it is unexpected that DC migration in steady state is only marginally inhibited. This might imply that the tightly regulated coordination of migDC migration speed holds information itself, which is read by T cells and codetermines their activation state as indicated by a diminished T cell response in EAE and a model of allergic contact dermatitis. Because generation of T cell responses in both preclinical

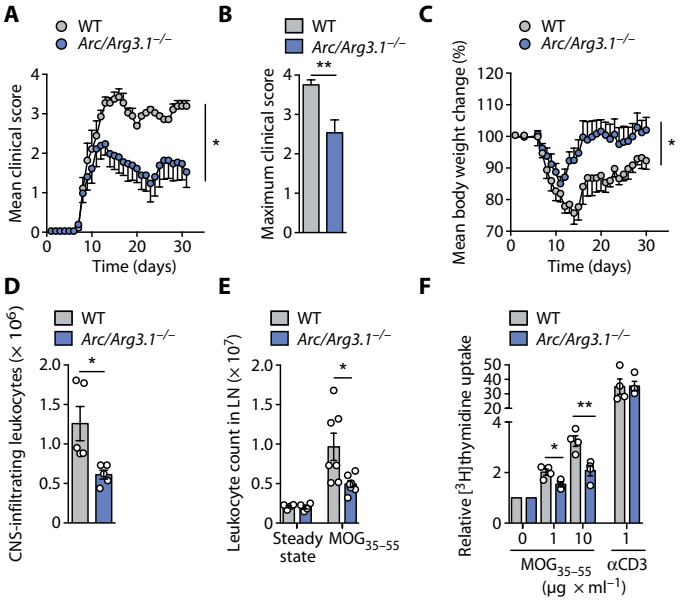

Fig. 6. Functional impact of Arc/Arg3.1 on T cell stimulation and EAE. (**A** to **C**) Mean clinical score, maximum clinical score, and mean body weight changes for EAE groups (n = 6 per genotype). Data from one of three experiments. Mean ± SEM. (A and C) Two-way ANOVA and (B) two-tailed Student's t test; $^*P < 0.05$, $^{**}P < 0.01$. (**D**) CNS-infiltrating immune cells at the peak (day 14) of EAE (n = 5 per genotype). Data from one of three experiments. Mean ± SEM. Two-tailed Student's t test; $^*P < 0.05$. (**E**) Absolute leukocyte count from sdLNs in steady state (n = 4 per genotype) and draining LNs 8 days after immunization (n = 7 per genotype) by flow cytometry. Data from one of three experiments. Mean ± SEM. Two-tailed Student's t test; $^*P < 0.05$. (**F**) T cell proliferation by [methyl-^{3}H]thymidine incorporation 8 days after immunization and restimulation with $MOG_{35–55}$ peptide or anti-CD3 ex vivo (n = 4 each genotype). Data from one of three experiments. Mean ± SEM. Two-tailed Student's t test; $^*P < 0.05$, $^{**}P < 0.01$.

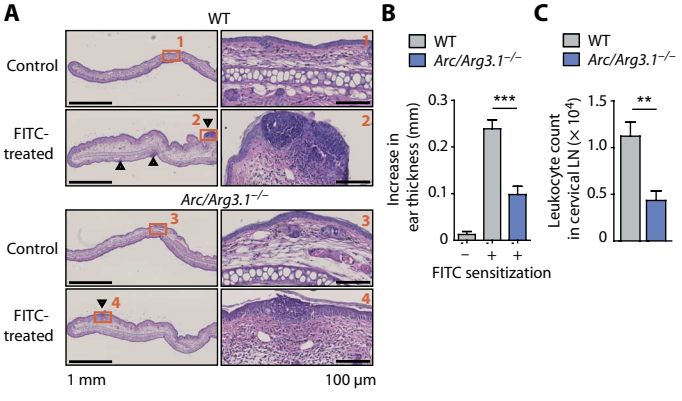

Fig. 7. Arc/Arg3.1-dependent skin-DC migration contributes to contact hypersensitivity. (**A** to **C**) Skin contact hypersensitivity was induced with 1% FITC in WT and *Arc/Arg3.1*$^{-/-}$ mice (n = 5 per genotype). (A) Representative images of hematoxylin and eosin–stained ears of respective genotypes. (B) Statistical analysis of increase in ear thickness of the antigen-treated ear compared with that of the vehicle-treated contralateral ear 24 hours after challenge. Data from one of two experiments. Mean ± SEM. Two-tailed Student's t test; $^{***}P < 0.001$. (C) Absolute leukocyte counts from draining cervical LNs. Data from one of two experiments. Mean ± SEM. Two-tailed Student's t test; $^{**}P < 0.01$.

models essentially depends on antigen presentation in the LNs by recently migrated skin-DCs (*43*, *44*), we assume that *Arc/Arg3.1* knockout (KO) mice show a general deficit in T cell activation toward any inflammatory antigen challenge introduced onto or into the skin. In this context, it has become apparent that distinct skin-DC subsets are pivotal for mounting T cell responses in different inflammatory scenario. For example, CD103$^+$ migDCs have been shown to induce encephalitogenic CD4$^+$ T cells after subcutaneous immunization with $MOG_{33–55}$ in CFA (*44*), which is in line with our finding of reduced CD103$^+$ migDCs with unaltered LCs and CD11b$^+$ migDCs in *Arc/Arg3.1* KO mice after subcutaneous immunization that results in insufficient CD4$^+$ T cell priming.

However, our study has limitations and leaves several questions unresolved. Although our studies demonstrate strongly impaired skin-DC migration in the absence of *Arc/Arg3.1* in FITC ear painting and drastically reduced allergic contact dermatitis reaction, which are two alternative models that have been shown to rely on different skin-DC subsets other than CD103$^+$ migDCs, particularly epidermal LCs and dermal Langerin$^+$ DCs (*9*), we have not formally proven that migration in these subsets also depends on Arc/Arg3.1. However, in agreement with the assumption of a broader impact of Arc/Arg3.1 on inflammatory migration in other skin-DC subsets including LCs, we can show that Arc/Arg3.1 is expressed in all migratory skin-DC subsets, and we observed broad migratory and morphological defects in BMDCs. Furthermore, epidermal LCs of *Arc/Arg3.1* KO mice showed morphological defects in situ, making functional dependency on Arc/Arg3.1 highly likely. Therefore, additional studies will have to determine the impact of Arc/Arg3.1 on inflammatory migration of each skin-DC subset in more detail and clarify the existence and possible functions of Arc/Arg3.1$^+$ migDCs at other host-environment interfaces, that is, the lung and the intestine. In addition, technical limitations prevented the use of freshly isolated primary migDCs in our in vitro migratory assays. Therefore, we had to rely on BMDCs, which contain various DC subsets (*31*), among those migDCs that show clear migratory capacities (*18*, *30*). In the future, it will be important to establish in vitro migration assays, which can be used with low numbers of freshly isolated migDCs. Moreover, during inflammation, we observed unaltered numbers of resident lymphoid tissue cDCs, although it is believed that some LN-"resident" cDCs are activated by invasion of highly activated migDCs from the surrounding tissue (*16*). This might be explained by rapid replenishment via the bloodstream (*45*), but this was not directly resolved in our study.

The coordination of DC subsets and the timing of LN arrival resemble the intricate cellular interactions and signaling networks in the nervous system, in which signal quality and the timing and processing of input signals determine the output, such as neuronal memory formation in which Arc/Arg3.1 is fundamentally involved (*21*, *46*). At the same time, this highlights the importance of our finding because targeting the migDC-specific Arc/Arg3.1 molecule or modifying other means of slowing DC migration or antigen delivery could offer therapeutic possibilities in aberrant immune responses or immunotherapy (*47*). The importance of proper DC migration for generating T cell responses in humans is best illustrated by an increase in susceptibility to tuberculosis in carriers of an *ASAP1* gene variant, which results in impaired DC migration (*48*). Thus, migration represents one of the important factors dictating successful pathogen responses and vaccine efficacy. Selectively

pulsing Arc/Arg3.1^{+} migDCs, which show superior migratory capacity, might allow a more efficient antigen delivery in subcutaneous or intradermal vaccination strategies for immunotherapies of patients with chronic infections (*49*) or tumors (*50*).

Moreover, we adopt a recently formulated need for a function-driven DC classification (*9*). In this context, in the skin, Arc/Arg3.1 functions as a suitable marker that defines the subset of migrating DCs on the basis of their migratory ability and not on unstable cell surface markers. This is in line with a proposed functional classification for other specialized DC subsets such as XCR1 for cross-presenting DCs (*51*). More controversy exists on whether recently identified transcription factors (*15*) and transcriptional networks can reveal DC subset specialization by ontogeny (*17*, *31*, *52*). However, this approach neglects the immanent high potential of DCs to adopt and change in response to microenvironmental changes and tissue-specific transcriptional imprinting (*53*). Defining functional DC subsets is highly relevant for clinical translation because ex vivo antigen-pulsed DCs are already in clinical use, for example, as a cancer vaccine (*54*). Preselecting DCs with advanced migratory capacities will likely enhance vaccination efficacy.

Together, we show that the "neuronal" protein Arc/Arg3.1 is required for fast DC migration because it facilitates actin remodeling in response to inflammatory stimuli and enables the identification of migrating DCs in the skin via their exclusive expression of Arc/Arg3.1 that might be used for DC-based immunotherapy (*47*).

MATERIALS AND METHODS

Study design

The aim of this study was to characterize and elucidate the molecular, cellular, and immunological role of Arc/Arg3.1 in DC migration from the skin to dLNs. The experimental design involved histologic, cellular, and biofluidic analyses using cells and tissues from WT with paired age- and sex-matched *Arc/Arg3.1* loss-of-function mutations in mice. To ensure adequate power to detect an effect size, the effect size was first calculated on the basis of pilot experiments and then used in power analysis. For analysis of in vivo immunological implications of *Arc/Arg3.1* loss of function, we performed preliminary experiments to determine requirements for sample size to minimize animal numbers. Animals were assigned randomly to EAE and allergic contact dermatitis experimental groups, and experiments were performed blinded to genotype and/or condition. When possible, the rater was also blinded to genotype or condition in all forms of data analysis. All experiments were approved by the local ethics committee (Behörde für Soziales, Familie, Gesundheit und Verbraucherschutz in Hamburg; G68/11, G15/081, and Org713).

Mice

We purchased C57BL/6 mice from the Jackson Laboratory, and *Arc/Arg3.1*$^{-/-}$ mice (*46*), *Ccr7*$^{-/-}$ mice (*26*), *Arc/Arg3.1*^{eGFP} mice (*25*, *55*), and 2D2 transgenic mice (*37*) were previously described. We held the mice under pathogen-free conditions. We used gender- and age-matched mice between 6 and 14 weeks of age for each experiment, with respective littermate control mice on a C57BL/6 background.

Cell preparation and culture condition

We isolated cells from the CNS, spleen, and bone marrow, as previously described (*36*, *56*). We obtained DCs from sdLNs by first mechanically disrupting the tissue before digesting it in collagenase D (1.25 mg ml^{-1}; Roche) and deoxyribonuclease I (50 μg ml^{-1}; Roche) for 35 min and gently shaking it at 37°C, adding 10 μM EDTA (Sigma-Aldrich) for the last 5 min. After homogenizing the tissue through a 40-μm cell strainer (BD Biosciences) and washing it with ice-cold phosphate-buffered saline (PBS), we pelleted cells (300*g* for 7 min at 4°C). For cell culturing, we used complete medium [10% fetal calf serum, 50 μM 2-mercaptoethanol, and penicillin/streptomycin (100 U ml^{-1}) in RPMI 1640]. Stimulation with LPS (100 ng ml^{-1}) was performed for 30 min, unless stated differently.

Generation of BMDCs

We obtained bone marrow from 6- to 12-week-old mice as described previously (*57*). Briefly, cells were homogenized through 40-μm cell strainers (BD Biosciences) and incubated in red blood cell lysis buffer (0.15 M NH_4Cl, 10 mM $KHCO_3$, and 0.1 mM Na_2EDTA in double-distilled H_2O at pH 7.4) for 5 min. We cultured the remaining cells in 100-ml cell culture flasks (Sarstedt) in mouse complete medium containing granulocyte-macrophage colony-stimulating factor (GM-CSF; 20 ng ml^{-1}) (PeproTech). We changed the medium every other day by carefully replacing the supernatant with fresh medium containing GM-CSF (20 ng ml^{-1}). We harvested semiadherent BMDCs on day 7, unless stated differently. For microchannel analysis only, we prepared BMDCs as described previously (*30*).

Inhibition of DC migration in vivo

We added fingolimod hydrochloride (FTY720; 3.5 μg ml^{-1}) (Sigma-Aldrich) to the drinking water of C57BL/6 or *Arc/Arg3.1*^{eGFP} mice (*27*) for 7 days before anesthetizing and killing them to analyze sdLNs. For recovery, we discontinued FTY720 treatment after 7 days in a different group of mice and fed normal drinking water for 7 consecutive days before anesthetizing and killing the mice to analyze sdLNs.

In vivo DC migration

We anesthetized mice for 5 min and painted their ears with 30 μl of 1% FITC (Sigma-Aldrich) in a carrier solution of acetone/dibutyl phthalate (1:1; Sigma-Aldrich and J. T. Barker) adapted from (*27*, *58*). After 20 hours, we collected dLNs and nondraining inguinal LNs and obtained single-cell suspensions, as described above. They were stained for CD11c and analyzed by flow cytometry after LIVE/DEAD staining.

Competitive DC migration in vivo

We concentrated BMDCs of respective genotypes at 2 × 10^7 cells ml^{-1} in PBS and labeled them with either 2.5 μM carboxyfluorescein succinimidyl ester (CFSE; Invitrogen) or 2.5 μM eFluor670 (eBioscience) for 10 min at 37°C before stopping the reaction with 5× volume of ice-cold mouse complete medium for 5 min on ice. We stimulated BMDCs with LPS (100 ng ml^{-1}) for 30 min at 37°C, washed them twice, mixed them in equal numbers, and adjusted the cells to a concentration of 6 × 10^7 cells ml^{-1}. To rule out any dye-specific effects, in each experiment, cells from both genotypes were labeled vice versa, and a third mix with cells labeled in both colors was added as control. After checking the actual input ratio of labeled cells by flow cytometry, we injected 20 μl of the mix in the footpad of C57BL/6 mice. After 18 hours, we collected the draining popliteal and nondraining inguinal LNs and analyzed migrated cells by flow cytometry. For each genotype, we calculated

the homing index (*59*) as a ratio of $CFSE^{+}_{LN}/eFlour670^{+}_{LN}$ to $CFSE^{+}_{input}/eFlour670^{+}_{input}$ to determine relative migratory capacity.

Migration speed measurement in microchannels

We prepared microchannels as described previously (*60*). Briefly, polydimethylsiloxane (PDMS) (GE Silicones) was used to prepare 8-μm by 5-μm microchannels. We coated their surface with bovine plasma fibronectin (10 μg ml^{-1}; Sigma) for 1 hour and then washed the surface three times with PBS before seeding of 1×10^5 BMDCs in complete medium supplemented with GM-CSF (50 ng ml^{-1})–containing supernatant obtained from transfected J558 cells. We imaged migrating BMDCs for 16 hours on an epifluorescence video microscope Nikon TiE equipped with a cooled charge-coupled device camera (HQ2, Photometrics) with an objective of 10×. A frequency of acquisition of one image per 2 min of transmission phase was used. We generated kymographs of the migrating cells by subtracting the mean projection of the whole movie to each frame, generating clear objects in dark background that were analyzed using a custom program, as we described previously (*30*). Blebbistatin (Tocris) was used at a concentration of 50 μM.

Actin distribution during migration

We performed DC migration in microchannels as described previously. The cells were fixed using 4% paraformaldehyde (PFA) after 16 hours of migration. We removed PDMS, favoring the accessibility of cells to the medium. We stained the remaining glass-adherent migratory cells with phalloidin Alexa Fluor 546 and 4′,6-diamidino-2-phenylindole (DAPI; Life Technologies) to visualize the polymerized actin and the nucleus, respectively. We imaged the cells on an epifluorescence microscope (Nikon TiE; objective, 20×). Individual cells were cropped, aligned, and superposed to generate a mean projection representing the overall distribution of actin in cells migrating into the microchannels. For the statistical analysis of relative F-actin distribution in migrating cells, we calculated the intensity of phalloidin staining in the front (first thirds of the cell) and at the rear (the rest of the signal) on an individual cell level using ImageJ.

DC high-content image analysis

We harvested BMDCs on day 6, stimulated them with LPS (100 ng ml^{-1}) for 1 hour, and plated 1×10^5 cells per well on poly-D-lysin (10 ng ml^{-1}; Sigma)–precoated, 96-well μClear cell culture plates (Greiner Bio One). We stimulated BMDC with LPS (100 ng ml^{-1}), CCL19 (100 ng ml^{-1}), polyI:C (100 μg ml^{-1}), TNF-α (10 ng ml^{-1}), or GM-CSF (20 ng ml^{-1}) for 16 hours before fixing adherent cells with 4% PFA. After permeabilization with 0.1% Triton X-100, we stained the cells for 30 min with rhodamine phalloidin (Molecular Probes) in PBS containing 1% bovine serum albumin (BSA). Nuclear staining was performed with Hoechst 33258 (Invitrogen). We analyzed cells on an Opera High Content Imaging System, in combination with the Columbus Image Data Storage and Analysis System (PerkinElmer). Automated imaging was performed with an objective of 60× and a sublayout with 35 image fields per well (covering representative and defined parts of the wells), resulting in image acquisition rates of about 60 cells per well. The image analysis algorithm sequence was generated with Columbus building blocks.

Immunocytofluorescence of BMDCs

We harvested BMDCs on day 6 and cultured them on poly-D-lysin (10 ng ml^{-1}; Sigma)–precoated coverslips at a concentration of 2×10^5 ml^{-1} in the presence of LPS (100 ng ml^{-1}) in a 24-well plate for 16 hours. We fixed adherent BMDCs with 4% PFA. After permeabilization with 0.1% Triton X-100, we stained the cells for 30 min with rhodamine phalloidin (Molecular Probes) in PBS containing 1% BSA. Coverslips were placed on object slides and embedded in Immu-Mount (Thermo Scientific). We took Z-stack images of whole BMDCs with a predefined step size on a confocal laser scanning microscope (Zeiss LSM 700; objective, 40×). To determine cell volume, we reconstructed the cell bodies by three-dimensional rendering using Imaris software (Bitplane) and calculated the volumes by ImageJ software. Blinded to genotype, we obtained area, perimeter, and circularity ($4\pi \times \text{area} \times \text{perimeter}^{-2}$; range, 0 to 1) from maximum projections using ImageJ64 software.

Immunohistochemistry of LCs in ear skin

After depilating the ear skin, we cut off the ears, separated dorsal and ventral sheet manually, and incubated them in 10 μM EDTA in PBS for 1.5 hours before we fixed the tissue in 4% PFA. We blocked the tissue with 300 mM glycine, 3% FBS, and Fc-receptor block (1:1000 rat anti-mouse anti-CD16/CD32; clone 93, BioLegend) before immunostaining with MHC class II (1:100 rat anti-mouse I-A/I-E; clone M5/114.15.2, BioLegend) overnight at 4°C. We mounted the tissue in mounting medium containing DAPI, took images on a confocal laser scanning microscope, and obtained cell area and perimeter using ImageJ64 software. Circularity was calculated as described previously.

DC adhesion

We coated 96-well flat-bottom, non–tissue culture–treated plates with 100 μl of PBS containing 1% BSA (PAA Laboratories), bovine fibronectin (50 μg ml^{-1}; Sigma-Aldrich), or human fibronectin (50 μg ml^{-1}; Sigma-Aldrich) per well overnight at 37°C and performed assays with modifications from previous description (*61*). We harvested BMDCs and rested them in a serum-free medium containing GM-CSF (20 ng ml^{-1}) for 2 hours at 37°C. Meanwhile, we blocked the precoated plates with PBS containing 1% BSA for 1 hour at 37°C. We plated 200 μl from 1×10^6 cells ml^{-1} in complete mouse medium containing GM-CSF (20 ng ml^{-1}) and incubated them for 3 hours at 37°C. For all conditions, triplicates were performed. Nonadherent cells were removed by washing them three times with serum-free medium. We fixed adherent cells in 2% PFA in PBS, stained them with 0.1% crystal violet (Sigma-Aldrich) for 25 min at room temperature, and removed excess stain by running them under water. Before drying, stained cells were photographed for representative image using an inverted Olympus CKX41 microscope equipped with an Olympus live-view digital SLR camera E-330. We lysed air-dried cells in PBS containing 0.5% Triton X-100 (Carl Roth) overnight in the dark. We determined adherent cells by measuring optical density at 595 nm using a universal microplate analyzer (Fusion-Alpha FPHT, PerkinElmer).

Antigen uptake

We stimulated BMDCs with LPS (100 ng ml^{-1}) for 30 min and incubated stimulated and unstimulated controls at 1×10^6 cells ml^{-1} with FITC-dextran (1 mg ml^{-1}; Sigma-Aldrich) at either 4° or 37°C. After 2 hours, phagocytosis was stopped with ice-cold PBS, and flow cytometry analysis of fluorescence intensity in FITC was performed.

Calcium imaging in DC

We incubated BMDCs with 4 μM 4-Fluo AM (Life Technologies) for 15 min at 37°C and 15 min at room temperature before washing them three times with complete mouse medium. After spinning

cells down, we resuspended them in Hepes-buffered saline medium and measured emitted fluorescence at room temperature on a flow cytometer (excitation, 488 nm; detection, band-pass filter 530/30) before and after adding thapsigargin with a final concentration of 200 μM.

Gene array

For gene expression analysis, we incubated 1.5×10^6 BMDCs from WT and *Arc/Arg3.1*$^{-/-}$ mice for 30 min with medium or LPS (100 ng ml^{-1}), washed them three times with medium, and incubated the cells again in medium for 1 hour before pelleting ($n = 3$ per group). The array was performed on GeneChip Mouse Gene 2.0 ST (Affymetrix) and processed as previously described (*62*). We performed statistical analysis by moderated *t* test corrected for multiple comparisons using the Benjamini-Hochberg method and identified differentially expressed candidate genes by a fold change of ≥2 and a false discovery rate–corrected $P < 0.05$. The gene array data were deposited in the Gene Expression Omnibus database (accession number: GSE71937).

EAE induction

We induced EAE as previously described (*36*). Briefly, we immunized mice subcutaneously with 200 μg of $MOG_{35–55}$ (Schafer-N) emulsified in CFA (BD Difco) containing heat-inactivated *Mycobacterium tuberculosis* (BD Difco) at 4 mg ml^{-1} into two sites of the hind flanks, followed by intravenous injection of 200 ng of pertussis toxin (*Bordetella pertussis*; Merck Biosciences) in PBS, which was repeated 48 hours later. Blinded to genotype, we weighed and scored mice daily for clinical signs by the following system: 0, no clinical deficits; 1, tail weakness; 2, hindlimb paresis; 3, partial hindlimb paralysis; 3.5, full hindlimb paralysis; 4, full hindlimb paralysis and forelimb paresis; 5, premorbid or dead. We killed mice at a score ≥4.

T cell restimulation

For analysis of T cell proliferation, we immunized mice with $MOG_{35–55}$ in CFA (as described previously), prepared single-cell solutions from dLNs on day 8, and cultured triplicates of 2×10^5 leukocytes per well in 96-well plates in the presence of different concentrations of $MOG_{35–55}$ peptide or anti-CD3 (145-2C11, eBioscience). After 3 days, we pulsed the plates with 1 μCi [methyl-^{3}H]thymidine (Amersham) per well for 16 hours, before we harvested, spotted, and measured incorporation and calculated relative [methyl-^{3}H]thymidine uptake, as described previously (*36*).

Contact hypersensitivity

We sensitized mice with 100 μl of 1% FITC in a carrier solution of acetone/dibutyl phthalate (1:1) on their shaved abdomen. Nonsensitized mice were shaved only. After 5 days, ear thickness was measured, 10 μl of 1% FITC dissolved in acetone/dibutyl phthalate (1:1) was applied to the right ear, and the left ear (control) was treated with the carrier solution only. After 24 hours, the ears were fixed and stained with hematoxylin and eosin for histology. Increase in ear thickness was determined by measuring the degree of ear swelling of the antigen-treated right ear compared with that of the vehicle-treated contralateral ear 24 hours after challenge. Absolute leukocyte counts from right draining cervical LNs were obtained by flow cytometry using cell-counting beads.

Coculture of T cells and DCs

To determine the T cell–stimulating capacity of DCs, we pulsed BMDCs with $MOG_{35–55}$ peptide (10 μg ml^{-1}) for 2 hours at 37°C before we washed the remaining peptide with ice-cold PBS three times. Then, we cocultured triplicates of 3×10^4 $MOG_{35–55}$-pulsed BMDCs with 2×10^5 purified CD4$^+$ T cells (>95% purity after isolation with magnetic-activated cell sorting; Miltenyi Biotec) from the spleen of MOG-specific T cell receptor transgenic mice (2D2) (*37*) in 200 μl of mouse complete medium. For control, we cocultured the purified CD4$^+$ T cells with 3×10^4 PBS-pulsed BMDCs alone or in the presence of $MOG_{35–55}$ peptide (10 μg ml^{-1}). After 72 hours, we pulsed the cells with 1 μCi [methyl-^{3}H]thymidine (Amersham) per well for 16 hours, before we harvested, spotted, and measured incorporation of [methyl-^{3}H]thymidine uptake, as described previously.

Stimulation of BMDCs

We incubated 1×10^6 BMDCs of *Arc/Arg.1*^{eGFP} mice with ATP (250 μM, Sigma-Aldrich), CCL19 (200 ng ml^{-1}, PeproTech), CCL21 (200 ng ml^{-1}, PeproTech), calcium (1 μM, Sigma-Aldrich), glutamate (1 mM, Sigma-Aldrich), high–molecular weight polyI:C (10 μg ml^{-1}, InvivoGen), low–molecular weight polyI:C (10 μg ml^{-1}, InvivoGen), LPS (100 ng ml^{-1}, PeproTech), and TNF-α (10 ng ml^{-1}, PeproTech) for 2 and 4 hours. We analyzed stimulated cells in flow cytometry for *Arc/Arg3.1*-eGFP, CD40 and CD80 expression and calculated fold change relative to unstimulated control.

Phosphorylation of nonmuscle MyoII

We stimulated 1×10^6 BMDCs with LPS (100 ng ml^{-1}) or medium for 1 hour at 37°C. After incubation, cells were immediately fixed with equal volume of cytofix buffer (BD Bioscience) for 10 min at 37°C and permeabilized with Perm Buffer III for 30 min on ice (both BD Bioscience). We stained the cells with phosphomyosin light chain antibody (1:300, Cell Signaling 3672) and species-specific secondary antibody in Cy3 (1:500; Jackson ImmunoResearch 711-165-152). As control, we included unstained samples and samples stained with rabbit immunoglobulin G (1:300; Sigma-Aldrich) and secondary antibody. We acquired fluorescence intensity with flow cytometry.

RhoA activation

We seeded triplicates of 1.5×10^6 BMDCs in flat-bottom, 12-well plates precoated with 500 μl of PBS containing 1% BSA (PAA Laboratories) and human fibronectin (20 μg ml^{-1} per well; Sigma-Aldrich) overnight at 37 °C. After 1-hour incubation, we determined active RhoA by using a luminescence-based enzyme-linked immunosorbent assay (ELISA) kit containing antibodies that specifically recognize the guanosine 5′-triphosphate–bound fraction of the protein (G-LISA, Cytoskeleton). We proceeded according to the manufacturer's protocol. We adjusted protein concentration in lysates to 1 mg ml^{-1} and used 50 μg per triplicate. The kit included a standard that allowed us to generate quantitative results.

Immunoblot

We performed immunoblotting on whole-cell lysates. Equal protein amounts were subjected to SDS–polyacrylamide gel electrophoresis and transferred to nitrocellulose. After blocking, we incubated the membranes with antibodies directed to Arc/Arg3.1 (mouse, 1:4000; Worley Lab) as previously described (*63*), cofilin (mouse, 1:3000; #612144, BD Transduction Laboratories), phosphorylated cofilin (hSer 3-R, 1:3000; sc-12912-R, Santa Cruz Biotechnology), or actin (rabbit, 1:3000; Cell Signaling) overnight at 4°C,

and washed and incubated them with a species-specific secondary antibody (1:20,000 to 1:50,000; LI-COR Biosciences) for 1 hour at room temperature. Labeling was visualized using enhanced chemiluminescence (LI-COR Biosciences). Quantification was carried out by densitometry using ImageJ software. For uncropped immunoblots, see fig. S8.

qRT-PCR for measuring mRNA expression

We purified RNA with the RNeasy Mini or Micro Kit (Qiagen) and synthesized complementary DNA (cDNA) with RevertAid H Minus First Strand cDNA Synthesis Kit (Fermentas) and diluted cDNA to a 1:5 ratio in H_2O for analysis. For tissue lysates, we used QIAshredder (Qiagen) for homogenizing. For quantitative real-time polymerase chain reaction (qRT-PCR), we used TaqMan Gene Expression Assays (Life Technologies) and performed all analyses in triplicates: Mm01204954_g1 (mouse *Arc*, sample) and TATA-binding protein as endogenous control Mm00446971_m1 (mouse *tbp*, reference). In some qRT-PCRs, we used Universal ProbeLibrary from Roche with Arc/Arg3.1 (forward: GGTGAGCTGAAGCCACCAAT; reverse: TTCACTGGTATGAATCACTGCTG; Biomers), and data were normalized to β-actin (05046190001). We analyzed all samples with a 7900HT Fast Real-Time PCR System (Applied Biosystems) and used Sequence Detection System v2.4 and RQ Manager software for analysis. Gene expression of genes of interest was calculated as $2^{-\Delta CT}$ relative to *Tbp* and β-*actin* or calculated as $2^{-\Delta\Delta CT}$ relative to mean *Arc/Arg3.1* expression of three individual WT brain lysates (hippocampus and cortex).

Immunohistochemistry

We anesthetized mice with an intraperitoneal injection of a solution of 10 μl g^{-1} of body weight [esketamine hydrochloride (10 mg ml^{-1}), xylazine hydrochloride (1.6 mg ml^{-1}), and water]. Afterward, we perfused the mice with 0.1 M phosphate buffer and fixed the tissue with 4% PFA. We resected the skin and postfixed it in 4% PFA overnight. We dehydrated the tissue with an ascending alcohol series and xylol, cast it in paraffin, and cut it on a vibratome in 3-μm-thick transversal sections. We performed antigen retrieval with an EDTA buffer and incubated the slides for 1 hour with an anti-CD11c antibody (1:100; ab33483, Abcam). As secondary antibody, we used Fast Red–conjugated anti-Armenian hamster (1:300). We analyzed the sections with a Leica DMD108 microscope and quantified the number of $CD11c^+$ cells by taking multiple representative images of 10 to 13 fields of view (0.08 mm^2) per animal with a ×40 lens and by counting them manually.

Flow cytometry

We incubated single-cell suspensions of mouse immune cells with antibody for 30 min at 4°C. We minimized nonspecific Fc receptor–mediated antibody binding by routine blocking with anti-mouse CD16/32 (93, eBioscience). The following antibodies were used: CD3 (145-2C11, BioLegend), CD3 (500A2, BD Biosciences), CD4 (GK1.5 and RM4-5, eBioscience), CD8a (53-6.7, BioLegend), CD11b (M1/70, BioLegend), CD11c (N418, eBioscience), CD19 (6D5, BioLegend), CD24 (M1/69, BioLegend), CD40 (3/23, BioLegend), CD45 (30F11, BioLegend), CD45R (RA3-6B2, eBioscience), CD49e (5H10-27, BioLegend), CD103 (2E7, BioLegend), CD207 (4C7, BioLegend), CD29 (HMβ1-1, BioLegend), CD80 (16-10A1, BioLegend), CD86 (GL-1, BioLegend), CD115 (AFS98, eBioscience), CD117 (2B8, BioLegend), CD135 (A2F10, BioLegend), CCR7 (4B12, BioLegend), GR1 (RB6-8C5, eBioscience), Ly-6G (1A8, BD Biosciences), MHCII (M5/114.15.2, BioLegend), NK1.1 (PK136, eBioscience), and PDCA-1 (129C1, BioLegend). We excluded dead cells from the analysis by staining with LIVE/DEAD Fixable Aqua or Near-IR Dead Cell Stain Kit (Life Technologies) following the manufacturer's protocols. For the determination of absolute cell numbers, $CD45^+$ leukocytes were quantified using Trucount beads (BD Biosciences). We obtained data using a BD LSR II flow cytometer (BD Biosciences) and analyzed them by using FlowJo (Tree Star) and FACSDiva (BD Biosciences). When possible, the rater was blinded to genotype or condition. Cell sorting was performed on BD FACS ARIA IIIu (BD Biosciences).

Immune cell identification strategies

For flow cytometry analysis and fluorescent cell sorting, we identified immune cell subsets in the sdLN and spleen (unless depicted differently) from live $CD45^+$ singlets: B cells ($CD19^+CD3^-$), T cells ($CD3^+CD19^-$), DCs ($CD11c^+CD19^-CD3^-$), migratory DCs ($SSC^{high}FSC^{high}MHCII^{high}CD11c^{inter}$), cDCs ($SSC^{high}FSC^{high}CD11c^{high}MHCII^{inter}$), pDCs ($CD11c^{inter}PDCA1^+$), and lymphocytes ($FSC^{low}SSC^{low}$ autofluorescence$^{neg}CD45^+CD11c^-$). For gating strategies, see fig. S9.

Statistical analysis

We performed all statistical tests using GraphPad Prism or R bioconductor. Most values are expressed as means ± SEM, unless stated differently. Where indicated, we analyzed for significance by using analysis of variance (ANOVA) with appropriate post hoc analysis for multiple groups, via a two-sided Student's *t* test or the Mann-Whitney test. Moderated *F* test and the Benjamini-Hochberg method were used for bioinformatics. We considered $^*P < 0.05$ as significant and $^{**}P < 0.01$ and $^{***}P < 0.001$ as highly significant. Original exact values for each data point in the presented figures can be gathered from table S2.

SUPPLEMENTARY MATERIALS

immunology.sciencemag.org/cgi/content/full/1/3/eaaf8665/DC1

Fig. S1. *Arc/Arg3.1* is expressed in various migDC subsets.
Fig. S2. Unaltered immune cells and progenitors in *Arc/Arg3.1*$^{-/-}$ mice.
Fig. S3. Arc/Arg3.1 does not influence antigen uptake, maturation, or calcium signaling in DCs.
Fig. S4. Normal distribution of integrins in the absence of *Arc/Arg3.1*.
Fig. S5. Arc/Arg3.1 is not induced by DC stimulation and has no influence on cofilin phosphorylation.
Fig. S6. Ameliorated EAE disease course but normal T cell stimulation in the absence of Arc/Arg3.1.
Fig. S7. Graphical summary of our findings.
Fig. S8. Uncropped immunoblots.
Fig. S9. Flow cytometry gating strategies.
Table S1. BMDC microarray data.
Table S2. Exact values.

REFERENCES AND NOTES

1. A. Iwasaki, R. Medzhitov, Control of adaptive immunity by the innate immune system. *Nat. Immunol.* **16**, 343–353 (2015).
2. J. Banchereau, R. M. Steinman, Dendritic cells and the control of immunity. *Nature* **392**, 245–252 (1998).
3. D. Ganguly, S. Haak, V. Sisirak, B. Reizis, The role of dendritic cells in autoimmunity. *Nat. Rev. Immunol.* **13**, 566–577 (2013).
4. D. H. Kaplan, B. Z. Igyártó, A. A. Gaspari, Early immune events in the induction of allergic contact dermatitis. *Nat. Rev. Immunol.* **12**, 114–124 (2012).
5. M. Baratin, C. Foray, O. Demaria, M. Habbeddine, E. Pollet, J. Maurizio, C. Verthuy, S. Davanture, H. Azukizawa, A. Flores-Langarica, M. Dalod, T. Lawrence, Homeostatic NF-κB signaling in steady-state migratory dendritic cells regulates immune homeostasis and tolerance. *Immunity* **42**, 627–639 (2015).

6. N. S. Wilson, L. J. Young, F. Kupresanin, S. H. Naik, D. Vremec, W. R. Heath, S. Akira, K. Shortman, J. Boyle, E. Maraskovsky, G. T. Belz, J. A. Villadangos, Normal proportion and expression of maturation markers in migratory dendritic cells in the absence of germs or Toll-like receptor signaling. *Immunol. Cell Biol.* **86**, 200–205 (2008).
7. M. L. Heuzé, P. Vargas, M. Chabaud, M. Le Berre, Y.-J. Liu, O. Collin, P. Solanes, R. Voituriez, M. Piel, A.-M. Lennon-Duménil, Migration of dendritic cells: Physical principles, molecular mechanisms, and functional implications. *Immunol. Rev.* **256**, 240–254 (2013).
8. Y. Belkaid, S. Tamoutounour, The influence of skin microorganisms on cutaneous immunity. *Nat. Rev. Immunol.* **16**, 353–366 (2016).
9. B. E. Clausen, P. Stoitzner, Functional specialization of skin dendritic cell subsets in regulating T cell responses. *Front. Immunol.* **6**, 534 (2015).
10. J.-P. Girard, C. Moussion, R. Förster, HEVs, lymphatics and homeostatic immune cell trafficking in lymph nodes. *Nat. Rev. Immunol.* **12**, 762–773 (2012).
11. C. A. Dendrou, L. Fugger, M. A. Friese, Immunopathology of multiple sclerosis. *Nat. Rev. Immunol.* **15**, 545–558 (2015).
12. M. Greter, F. L. Heppner, M. P. Lemos, B. M. Odermatt, N. Goebels, T. Laufer, R. J. Noelle, B. Becher, Dendritic cells permit immune invasion of the CNS in an animal model of multiple sclerosis. *Nat. Med.* **11**, 328–334 (2005).
13. E. J. McMahon, S. L. Bailey, C. V. Castenada, H. Waldner, S. D. Miller, Epitope spreading initiates in the CNS in two mouse models of multiple sclerosis. *Nat. Med.* **11**, 335–339 (2005).
14. M. Noordegraaf, V. Flacher, P. Stoitzner, B. E. Clausen, Functional redundancy of Langerhans cells and Langerin$^+$ dermal dendritic cells in contact hypersensitivity. *J. Invest. Dermatol.* **130**, 2752–2759 (2010).
15. M. Guilliams, F. Ginhoux, C. Jakubzick, S. H. Naik, N. Onai, B. U. Schraml, E. Segura, R. Tussiwand, S. Yona, Dendritic cells, monocytes and macrophages: A unified nomenclature based on ontogeny. *Nat. Rev. Immunol.* **14**, 571–578 (2014).
16. M. Merad, P. Sathe, J. Helft, J. Miller, A. Mortha, The dendritic cell lineage: Ontogeny and function of dendritic cells and their subsets in the steady state and the inflamed setting. *Annu. Rev. Immunol.* **31**, 563–604 (2013).
17. J. C. Miller, B. D. Brown, T. Shay, E. L. Gautier, V. Jojic, A. Cohain, G. Pandey, M. Leboeuf, K. G. Elpek, J. Helft, D. Hashimoto, A. Chow, J. Price, M. Greter, M. Bogunovic, A. Bellemare-Pelletier, P. S. Frenette, G. J. Randolph, S. J. Turley, M. Merad; Immunological Genome Consortium, Deciphering the transcriptional network of the dendritic cell lineage. *Nat. Immunol.* **13**, 888–899 (2012).
18. T. Lämmermann, B. L. Bader, S. J. Monkley, T. Worbs, R. Wedlich-Söldner, K. Hirsch, M. Keller, R. Förster, D. R. Critchley, R. Fässler, M. Sixt, Rapid leukocyte migration by integrin-independent flowing and squeezing. *Nature* **453**, 51–55 (2008).
19. B. T. Schaar, S. K. McConnell, Cytoskeletal coordination during neuronal migration. *Proc. Natl. Acad. Sci. U.S.A.* **102**, 13652–13657 (2005).
20. L. A. Cingolani, Y. Goda, Actin in action: The interplay between the actin cytoskeleton and synaptic efficacy. *Nat. Rev. Neurosci.* **9**, 344–356 (2008).
21. C. R. Bramham, P. F. Worley, M. J. Moore, J. F. Guzowski, The immediate early gene *Arc/Arg3.1*: Regulation, mechanisms, and function. *J. Neurosci.* **28**, 11760–11767 (2008).
22. E. Messaoudi, T. Kanhema, J. Soule, A. Tiron, G. Dagyte, B. da Silva, C. R. Bramham, Sustained Arc/Arg3.1 synthesis controls long-term potentiation consolidation through regulation of local actin polymerization in the dentate gyrus in vivo. *J. Neurosci.* **27**, 10445–10455 (2007).
23. W. Link, U. Konietzko, G. Kauselmann, M. Krug, B. Schwanke, U. Frey, D. Kuhl, Somatodendritic expression of an immediate early gene is regulated by synaptic activity. *Proc. Natl. Acad. Sci. U.S.A.* **92**, 5734–5738 (1995).
24. G. L. Lyford, K. Yamagata, W. E. Kaufmann, C. A. Barnes, L. K. Sanders, N. G. Copeland, D. J. Gilbert, N. A. Jenkins, A. A. Lanahan, P. F. Worley, *Arc*, a growth factor and activity-regulated gene, encodes a novel cytoskeleton-associated protein that is enriched in neuronal dendrites. *Neuron* **14**, 433–445 (1995).
25. S. Gong, C. Zheng, M. L. Doughty, K. Losos, N. Didkovsky, U. B. Schambra, N. J. Nowak, A. Joyner, G. Leblanc, M. E. Hatten, N. Heintz, A gene expression atlas of the central nervous system based on bacterial artificial chromosomes. *Nature* **425**, 917–925 (2003).
26. R. Förster, A. Schubel, D. Breitfeld, E. Kremmer, I. Renner-Müller, E. Wolf, M. Lipp, CCR7 coordinates the primary immune response by establishing functional microenvironments in secondary lymphoid organs. *Cell* **99**, 23–33 (1999).
27. N. Czeloth, G. Bernhardt, F. Hofmann, H. Genth, R. Förster, Sphingosine-1-phosphate mediates migration of mature dendritic cells. *J. Immunol.* **175**, 2960–2967 (2005).
28. L. Kappos, E.-W. Radue, P. O'Connor, C. Polman, R. Hohlfeld, P. Calabresi, K. Selmaj, C. Agoropoulou, M. Leyk, L. Zhang-Auberson, P. Burtin; FREEDOMS Study Group, A placebo-controlled trial of oral fingolimod in relapsing multiple sclerosis. *N. Engl. J. Med.* **362**, 387–401 (2010).
29. B. U. Schraml, J. van Blijswijk, S. Zelenay, P. G. Whitney, A. Filby, S. E. Acton, N. C. Rogers, N. Moncaut, J. J. Carvajal, C. Reis e Sousa, Genetic tracing via DNGR-1 expression history defines dendritic cells as a hematopoietic lineage. *Cell* **154**, 843–858 (2013).
30. G. Faure-André, P. Vargas, M.-I. Yuseff, M. Heuze, J. Diaz, D. Lankar, V. Steri, J. Manry, S. Hugues, F. Vascotto, J. Boulanger, G. Raposo, M.-R. Bono, M. Rosemblatt, M. Piel, A.-M. Lennon-Duménil, Regulation of dendritic cell migration by CD74, the MHC class II-associated invariant chain. *Science* **322**, 1705–1710 (2008).
31. J. Helft, J. Böttcher, P. Chakravarty, S. Zelenay, J. Huotari, B. U. Schraml, D. Goubau, C. Reis a Sousa, GM-CSF mouse bone marrow cultures comprise a heterogeneous population of CD11c$^+$MHCII$^+$ macrophages and dendritic cells. *Immunity* **42**, 1197–1211 (2015).
32. E. H. J. Danen, P. Sonneveld, C. Brakebusch, R. Fässler, A. Sonnenberg, The fibronectin-binding integrins $\alpha5\beta1$ and $\alpha v\beta3$ differentially modulate RhoA–GTP loading, organization of cell matrix adhesions, and fibronectin fibrillogenesis. *J. Cell Biol.* **159**, 1071–1086 (2002).
33. P. Vargas, P. Maiuri, M. Bretou, P. J. Sáez, P. Pierobon, M. Maurin, M. Chabaud, D. Lankar, D. Obino, E. Terriac, M. Raab, H.-R. Thiam, T. Brocker, S. M. Kitchen-Goosen, A. S. Alberts, P. Sunareni, S. Xia, R. Li, R. Voituriez, M. Piel, A.-M. Lennon-Duménil, Innate control of actin nucleation determines two distinct migration behaviours in dendritic cells. *Nat. Cell Biol.* **18**, 43–53 (2016).
34. J. J. Bravo-Cordero, M. A. O. Magalhaes, R. J. Eddy, L. Hodgson, J. Condeelis, Functions of cofilin in cell locomotion and invasion. *Nat. Rev. Mol. Cell Biol.* **14**, 405–415 (2013).
35. M. Chabaud, M. L. Heuzé, M. Bretou, P. Vargas, P. Maiuri, P. Solanes, M. Maurin, E. Terriac, M. Le Berre, D. Lankar, T. Piolot, R. S. Adelstein, Y. Zhang, M. Sixt, J. Jacobelli, O. Bénichou, R. Voituriez, M. Piel, A.-M. Lennon-Duménil, Cell migration and antigen capture are antagonistic processes coupled by myosin II in dendritic cells. *Nat. Commun.* **6**, 7526 (2015).
36. B. Schattling, K. Steinbach, E. Thies, M. Kruse, A. Menigoz, F. Ufer, V. Flockerzi, W. Brück, O. Pongs, R. Vennekens, M. Kneussel, M. Freichel, D. Merkler, M. A. Friese, TRPM4 cation channel mediates axonal and neuronal degeneration in experimental autoimmune encephalomyelitis and multiple sclerosis. *Nat. Med.* **18**, 1805–1811 (2012).
37. E. Bettelli, M. Pagany, H. L. Weiner, C. Linington, R. A. Sobel, V. K. Kuchroo, Myelin oligodendrocyte glycoprotein–specific T cell receptor transgenic mice develop spontaneous autoimmune optic neuritis. *J. Exp. Med.* **197**, 1073–1081 (2003).
38. C. L. Peebles, J. Yoo, M. T. Thwin, J. J. Palop, J. L. Noebels, S. Finkbeiner, Arc regulates spine morphology and maintains network stability in vivo. *Proc. Natl. Acad. Sci. U.S.A.* **107**, 18173–18178 (2010).
39. M. Murrell, P. W. Oakes, M. Lenz, M. L. Gardel, Forcing cells into shape: The mechanics of actomyosin contractility. *Nat. Rev. Mol. Cell Biol.* **16**, 486–498 (2015).
40. T. Lämmermann, R. N. Germain, The multiple faces of leukocyte interstitial migration. *Semin. Immunopathol.* **36**, 227–251 (2014).
41. E. Frittoli, G. Matteoli, A. Palamidessi, E. Mazzini, L. Maddaluno, A. Disanza, C. Yang, T. Svitkina, M. Resciano, G. Scita, The signaling adaptor Eps8 is an essential actin capping protein for dendritic cell migration. *Immunity* **35**, 388–399 (2011).
42. Y. Yamakita, F. Matsumura, M. W. Lipscomb, P.-c. Chou, G. Werlen, J. K. Burkhardt, S. Yamashiro, Fascin1 promotes cell migration of mature dendritic cells. *J. Immunol.* **186**, 2850–2859 (2011).
43. A. A. Itano, S. J. McSorley, R. L. Reinhardt, B. D. Ehst, E. Ingulli, A. Y. Rudensky, M. K. Jenkins, Distinct dendritic cell populations sequentially present antigen to CD4 T cells and stimulate different aspects of cell-mediated immunity. *Immunity* **19**, 47–57 (2003).
44. I. L. King, M. A. Kroenke, B. M. Segal, GM-CSF–dependent, CD103$^+$ dermal dendritic cells play a critical role in Th effector cell differentiation after subcutaneous immunization. *J. Exp. Med.* **207**, 953–961 (2010).
45. H. Nakano, K. L. Lin, M. Yanagita, C. Charbonneau, D. N. Cook, T. Kakiuchi, M. D. Gunn, Blood-derived inflammatory dendritic cells in lymph nodes stimulate acute T helper type 1 immune responses. *Nat. Immunol.* **10**, 394–402 (2009).
46. N. Plath, O. Ohana, B. Dammermann, M. L. Errington, D. Schmitz, C. Gross, X. Mao, A. Engelsberg, C. Mahlke, H. Welzl, U. Kobalz, A. Stawrakakis, E. Fernandez, R. Waltereit, A. Bick-Sander, E. Therstappen, S. F. Cooke, V. Blanquet, W. Wurst, B. Salmen, M. R. Bösl, H.-P. Lipp, S. G. N. Grant, T. V. P. Bliss, D. P. Wolfer, D. Kuhl, Arc/Arg3.1 is essential for the consolidation of synaptic plasticity and memories. *Neuron* **52**, 437–444 (2006).
47. K. Palucka, J. Banchereau, I. Mellman, Designing vaccines based on biology of human dendritic cell subsets. *Immunity* **33**, 464–478 (2010).
48. J. Curtis, Y. Luo, H. L. Zenner, D. Cuchet-Lourenço, C. Wu, K. Lo, M. Maes, A. Alisaac, E. Stebbings, J. Z. Liu, L. Kopanitsa, O. Ignatyeva, Y. Balabanova, V. Nikolayevskyy, I. Baessmann, T. Thye, C. G. Meyer, P. Nurnberg, R. D. Horstmann, F. Drobniewski, V. Plagnol, J. C. Barrett, S. Nejentsev, Susceptibility to tuberculosis is associated with variants in the *ASAP1* gene encoding a regulator of dendritic cell migration. *Nat. Genet.* **47**, 523–527 (2015).
49. F. García, N. Climent, A. C. Guardo, C. Gil, A. León, B. Autran, J. D. Lifson, J. Martínez-Picado, J. Dalmau, B. Clotet, J. M. Gatell, M. Plana, T. Gallart; DCV2/MANONO7-ORVACS Study Group, A dendritic cell–based vaccine elicits T cell responses associated with control of HIV-1 replication. *Sci. Transl. Med.* **5**, 166ra162 (2013).
50. D. A. Mitchell, K. A. Batich, M. D. Gunn, M.-N. Huang, L. Sanchez-Perez, S. K. Nair, K. L. Congdon, E. A. Reap, G. E. Archer, A. Desjardins, A. H. Friedman, H. S. Friedman,

J. E. Herndon II, A. Coan, R. E. McLendon, D. A. Reardon, J. J. Vredenburgh, D. D. Bigner, J. H. Sampson, Tetanus toxoid and CCL3 improve dendritic cell vaccines in mice and glioblastoma patients. *Nature* **519**, 366–369 (2015).
51. K. Crozat, S. Tamoutounour, T.-P. Vu Manh, E. Fossum, H. Luche, L. Ardouin, M. Guilliams, H. Azukizawa, B. Bogen, B. Malissen, S. Henri, M. Dalod, Cutting edge: Expression of XCR1 defines mouse lymphoid-tissue resident and migratory dendritic cells of the CD8α^+ type. *J. Immunol.* **187**, 4411–4415 (2011).
52. A. Schlitzer, V. Sivakamasundari, J. Chen, H. R. Sumatoh, J. Schreuder, J. Lum, B. Malleret, S. Zhang, A. Larbi, F. Zolezzi, L. Renia, M. Poidinger, S. Naik, E. W. Newell, P. Robson, F. Ginhoux, Identification of cDC1- and cDC2-committed DC progenitors reveals early lineage priming at the common DC progenitor stage in the bone marrow. *Nat. Immunol.* **16**, 718–728 (2015).
53. B. Pulendran, The varieties of immunological experience: Of pathogens, stress, and dendritic cells. *Annu. Rev. Immunol.* **33**, 563–606 (2015).
54. B. M. Carreno, V. Magrini, M. Becker-Hapak, S. Kaabinejadian, J. Hundal, A. A. Petti, A. Ly, W.-R. Lie, W. H. Hildebrand, E. R. Mardis, G. P. Linette, A dendritic cell vaccine increases the breadth and diversity of melanoma neoantigen-specific T cells. *Science* **348**, 803–808 (2015).
55. S. Siegert, E. Cabuy, B. G. Scherf, H. Kohler, S. Panda, Y.-Z. Le, H. J. Fehling, D. Gaidatzis, M. B. Stadler, B. Roska, Transcriptional code and disease map for adult retinal cell types. *Nat. Neurosci.* **15**, 487–495 (2012).
56. K. Steinbach, M. Piedavent, S. Bauer, J. T. Neumann, M. A. Friese, Neutrophils amplify autoimmune central nervous system infiltrates by maturing local APCs. *J. Immunol.* **191**, 4531–4539 (2013).
57. K. Inaba, M. Inaba, N. Romani, H. Aya, M. Deguchi, S. Ikehara, S. Muramatsu, R. M. Steinman, Generation of large numbers of dendritic cells from mouse bone marrow cultures supplemented with granulocyte/macrophage colony-stimulating factor. *J. Exp. Med.* **176**, 1693–1702 (1992).
58. S. E. Macatonia, A. J. Edwards, S. C. Knight, Dendritic cells and the initiation of contact sensitivity to fluorescein isothiocyanate. *Immunology* **59**, 509–514 (1986).
59. J. R. Mora, M. R. Bono, N. Manjunath, W. Weninger, L. L. Cavanagh, M. Rosemblatt, U. H. von Andrian, Selective imprinting of gut-homing T cells by Peyer's patch dendritic cells. *Nature* **424**, 88–93 (2003).
60. P. Vargas, E. Terriac, A.-M. Lennon-Duménil, M. Piel, Study of cell migration in microfabricated channels. *J. Vis. Exp.* **21**, e51099 (2014).
61. D. R. Spurrell, N. A. Luckashenak, D. C. Minney, A. Chaplin, J. M. Penninger, R. S. Liwski, J. L. Clements, K. A. West, Vav1 regulates the migration and adhesion of dendritic cells. *J. Immunol.* **183**, 310–318 (2009).
62. S. Meyer, J. Nolte, L. Opitz, G. Salinas-Riester, W. Engel, Pluripotent embryonic stem cells and multipotent adult germline stem cells reveal similar transcriptomes including pluripotency-related genes. *Mol. Hum. Reprod.* **16**, 846–855 (2010).
63. L. Alberi, S. Liu, Y. Wang, R. Badie, C. Smith-Hicks, J. Wu, T. J. Pierfelice, B. Abazyan, M. P. Mattson, D. Kuhl, M. Pletnikov, P. F. Worley, N. Gaiano, Activity-induced Notch signaling in neurons requires *Arc/Arg3.1* and is essential for synaptic plasticity in hippocampal networks. *Neuron* **69**, 437–444 (2011).

Acknowledgments: We thank P. Worley (Johns Hopkins University, Baltimore, USA) for providing anti-Arc/Arg3.1 antibody, B. Roska (Friedrich Miescher Institute for Biomedical Research, Basel, Switzerland) for providing *Arc/Arg3.1*^{eGFP} mice, A.-M. Lennon-Duménil (Institut Curie, Paris, France) for support and helpful suggestions, and X. Mao (University Medical Center Hamburg-Eppendorf, Hamburg, Germany) for support with initial experimental procedures. We also thank the HEXT FACS sorting core unit (Universitätsklinikum Hamburg-Eppendorf) for flow cytometry sorting. **Funding:** This work was supported by the Boehringer Ingelheim Stiftung (Exploration Grant) and the Deutsche Forschungsgemeinschaft Emmy Noether-Programme (FR1720/3-1) to M.A.F. **Author contributions:** F.U. organized, designed, and performed most of the experimental work and data analysis and wrote the manuscript. P.V. performed microchannel migration experiments. J.B.E. performed bioinformatics and helped with experimental procedures and the writing of the manuscript. J.T., B.S., H.W., S.B., N.K., and A.W. helped with experimental procedures and data discussion. G.S.-R. carried out gene array analyses. O.K. and O.P. helped in DC morphology analysis. O.O. and D.K. provided *Arc/Arg3.1*$^{-/-}$ mice and participated in data discussion. M.A.F. designed the study, oversaw and directed the experiments, provided funding for the research, and wrote the manuscript. F.U., P.V., J.B.E., and M.A.F. conducted statistical analyses. **Competing interests:** The authors declare that they have no competing financial interests. **Data and materials availability:** The microarray data have been deposited in the Gene Expression Omnibus at the National Center for Biotechnology Information with accession no. GSE71937.

Submitted 13 April 2016
Accepted 24 August 2016
Published 23 September 2016
10.1126/sciimmunol.aaf8665

Citation: F. Ufer, P. Vargas, J. B. Engler, J. Tintelnot, B. Schattling, H. Winkler, S. Bauer, N. Kursawe, A. Willing, O. Keminer, O. Ohana, G. Salinas-Riester, O. Pless, D. Kuhl, M. A. Friese, Arc/Arg3.1 governs inflammatory dendritic cell migration from the skin and thereby controls T cell activation. *Sci. Immunol.* **1**, eaaf8665 (2016).

Science Immunology
AAAS

Arc/Arg3.1 governs inflammatory dendritic cell migration from the skin and thereby controls T cell activation

Friederike Ufer, Pablo Vargas, Jan Broder Engler, Joseph Tintelnot, Benjamin Schattling, Hana Winkler, Simone Bauer, Nina Kursawe, Anne Willing, Oliver Keminer, Ora Ohana, Gabriela Salinas-Riester, Ole Pless, Dietmar Kuhl and Manuel A. Friese

*Sci. Immunol.*1, eaaf8665 (2016)
doi: 10.1126/sciimmunol.aaf8665

Editor's Summary Dendritic cell migration reformDendritic cells are the messengers of the immune system, transporting antigens from sites of inflammation to the lymph organs that serve as central hubs for immune activation. Ufer et al. have identified a neuronal plasticity molecule--activity-regulated cytoskeleton-associated protein/activity-regulated gene 3.1 (Arc/Arg3.1)--that is expressed in migratory dendritic cells in the skin. Arc/Arg3.1 regulates cytoskeletal changes in dendritic cells, accelerating migration in response to inflammation. Moreover, Arc/Arg3.1 was required for inducing T cell responses in two different disease models--experimental autoimmune encephalitis and allergic contact dermatitis. Targeting Arc/Arg3.1 may therefore be a therapeutic strategy to modify dendritic cell immunotherapy.

Science Immunology (ISSN 2375-2548) publishes new articles weekly. The journal is published by the American Association for the Advancement of Science (AAAS), 1200 New York Avenue NW, Washington, DC 20005.